A matter of charge: Electrostatically tuned coassembly of amphiphilic peptides

*Elad Arad[1,2], Topaz Levi[3], Gal Yosefi[4], Itamar Kass[1], Ifat Cohen-Erez[3], Ziv Azoulay[3], Ronit Bitton[1,4], Raz Jelinek[1,2] and Hanna Rapaport[1,3]**

[1] Ilse Katz Institute (IKI) for Nanoscale Science and Technology
Ben-Gurion University of the Negev,
Beer-Sheva 8410501, Israel

[2] Department of Chemistry
Ben-Gurion University of the Negev,
Beer-Sheva 8410501, Israel.

[3] Avram and Stella Goldstein-Goren Department of Biotechnology Engineering
Ben Gurion University of the Negev,
Beer Sheva 8410501, Israel.

[4] Department of Chemical Engineering
Ben-Gurion University of the Negev,
Beer-Sheva 8410501, Israel.

*Author to whom correspondence should be addressed: Hannarap@bgu.ac.il

ABSTRACT

Coassembly of peptide biomaterials offers a compelling avenue to broaden the spectrum of hierarchically ordered supramolecular nanoscale structures that may be relevant for biomedical and biotechnological applications. In this study we present a comprehensive exploration of binary coassembly leveraging amphiphilic and oppositely charged, anionic and cationic, β-sheet peptides, which may give rise to a diverse range of coassembled forms. Mixtures of the peptides exhibit a notably diminished critical assembly concentration (CAC), in comparison to the

corresponding values of the pure peptides. Intriguingly, the sweet spot for coassembled fibril formation was found to require excess of the cationic peptide whereas equimolar mixtures of the peptides exhibited the maximum folding into β-sheet structures. Mixtures of the peptides coassembled sequentially from solutions at concentrations surpassing each peptide's intrinsic CAC, were also found to require a higher portion of the cationic peptide to stabilize hydrogels. This study illuminates a systematic exploration of complementary charged β-sheet peptides. The results may be relevant to the fundamental understanding of such intricate assembly systems and to the formulation of peptide-based nanostructures with diverse functionalities.

KEYWORDS: Peptide biomaterials, coassembly, charged peptides, β-sheet peptides, peptide hydrogels

Introduction

Biological systems can enhance their functionality by forming complex structures through precise and hierarchically ordered molecular assemblies. Recent studies have adopted a supramolecular approach to develop multi-component systems comprising of small molecules[1,2], polymers[3–5] and nanoparticles[6–8]. Peptides were designed as building blocks of synthetic nanomaterials with molecular precision and controllability resembling those found in nature[9,10]. The biological functionality of peptide and protein assemblies is strongly dependent on multiple intermolecular interactions[9,11–13] that are influenced by pH, ionic strength, specific small molecules, as well as on kinetic factors that may play a role during folding and stabilization[14–16]. The formation of designed β-sheet structures was demonstrated in various systems of peptides

with amphiphilic patterns of alternating polar and non-polar residues along the backbone[17–20]. The stacking of aromatic residues was also shown to contribute to hydrophobic interactions in β-sheet assemblies[21,22] and coiled-coil amphiphilic assemblies[23,24]. Peptides can also coassemble with nucleotides[25], sugars[26], polymers[27], inorganic nanoparticles[28,29], small molecules[30], and other proteins and peptides[31–33]. Peptide-polymers coassemblies were shown to form dynamic materials[34] with unique mechanisms of controlled drug release from molecular complexes[3] and gels[35]. Some of the inhibitors of amyloid aggregation can be considered disrupting agents through coassembly[36,37]. β-sheet peptides were found to coassemble with blood-clotting proteins in a manner that may be relevant to coagulation[38]. Coassemblies of ***peptide mixtures (PM)*** were explored with collagen-like short motifs[39,40], α-helical[41], and chiral dependent β-sheet structures[42–44]. These PM coassemblies exhibited various morphologies, like flat and twisted ribbons, sheets and fibrils[31,32]. Structurally tunable PM have shown increased peptide catalytic activity[45] and templating of amino-acid condensation[46], multi-strand catalytic activity by tripeptides[47], electron transfer reactions[48] and increased specificity[49]. Other PM were designed to incorporate integrin binding sequences to improve cell culture experiments[50,51].

One of the important forces that may govern the PM coassembly are electrostatic interactions. We have shown that such forces may play a prominent role in membrane-peptide interactions and enhance β-sheet assembly and fibrillation[52]. Additionally, several studies have tracked the initial steps of coassembly of anionic and cationic peptides under diluted conditions, showing that electrostatic interactions stabilize β-sheet oligomers and fibrils in a concentration-dependent fashion and in a microsecond timescale[53–55]. Multicomponent peptide hydrogels can be formed by mixtures of pH-responsive peptides with opposite charges[56–61]. Likewise, side-chain specificity was shown to influence the coassembly of charge-complementary β-sheet-forming

peptide pairs[54,62]. Although direct observation of the peptide distribution within oligomers is experimentally challenging, molecular dynamics predict that mixtures of such peptides do not necessarily coassemble into heteromeric oligomers but may also form homomeric ones[53].

In this study we systematically explored binary assemblies of two amphiphilic β-sheet peptides, displaying the same structural motif Pro-X-(Phe-X)$_5$-Pro, in which the backbone consists of hydrophilic amino acids (X) alternating with the hydrophobic, Phe, amino acid and the Pro termini were shown to induce β-sheet formation[63]. One of these is an anionic peptide with X = Asp, and the other is cationic with X = Lys, denoted An-FD and Cat-FK, respectively. An-FD was shown to assemble into β-sheet structures at the air-water interface, pointing the hydrophobic side-chains to the air and the acidic residues to the aqueous solution, and also form bilayer-fibril in solution[64–67]. This anionic peptide was previously shown to exhibit unique biologically relevant properties including the stabilization of a hydrogel phase at near neutral pH[15], induce biomineralization and bone tissue regeneration *in-vivo*[14,68], serve as a scaffold for cell culture[51] and drug delivery[66], and at certain concentrations retard blood clotting[38]. Cat-FK was designed for the generation of nanofiber gold mesh and later was employed in the formulation of drug-loaded nanoparticles that were found to effectively target drugs in cell culture and *in-vivo*, toward mitochondria [3,69–71]. Cat-FK was found to interact with anionic lipid bilayers[52] and at certain concentrations destabilize blood plasma[38]. Here we envisoned that zwitterionic assemblies of An-FD and Cat-FK could form coassemblies and possibly create stable hydrogels that will expand the realm of their potential biological applications. Hence we explore PM of An-FD and Cat-FK in different concentrations, below and above their critical assembly concentration (CAC) and at concentration that were expected to stabilize a hydrogel

phase, while also screening the effect of different pH values and mixing order to elucidate the structure and composition of the various mixtures.

Results and Discussion

Coassembly in solutions

CAC was measured for the pure peptides and for several of their PM compositions that comprise 25, 50 and 75 % An-FD, using 8-Anilino-1-naphthalenesulfonic acid (ANS) as a reporter of hydrophobic niches that are expected to be formed, upon assembly of these amphiphilic peptides (Figure 1A and Figure S1). The CACs of the pure An-FD and Cat-FK were found to be in the millimolar range, 2.3 and 10.1 mM, respectively. In contrast, the CAC values of the PM were much lower, 0.096, 0.058 and 0.14 mM for the 25, 50 and 75 % An-FD, respectively, as could be expected for peptides interacting by complementary electrostatic charges. The minimal CAC value that was detected for the PM with the 50 % An-FD, appeared to suit the expected 1:1 mol:mol ratio for most favorable electrostatic interactions. Next, the ANS fluorescence analysis was used to evaluate the hydrophobic niches presumed to be formed upon PM's coassembly, at a total concentration of 0.3 mM. At this concentration the pure peptides, both below their own CAC value, showed no significant increase in the ANS fluorescence (Figure 1B, samples 0 % and 100 %). The ANS of the 0.3 mM PM showed a bell-shaped behavior (Figure 1B) with a surprising maximum signal for the 40 % An-FD, rather than for the equal ratio of the two peptides. This unique behavior suggests that excess of Cat-FK may play a role in enhancing the solubility or dispersity of the PM coassemblies. The coassembly of these 0.3 mM PM was also evident by an increase in the turbidity of these solutions (Figure 1B inset and Figure S2). As a

control, a scrambled analog of An-FD, denoted Sc-FD (lacking the ability to adopt β-sheet conformation[38]), that was also mixed with Cat-FK under similar conditions, generated similar pattern of increased ANS fluorescence intensity, with a maximal at 40 % Sc-FD. The fact that both An-FD and Sc-FD show similar trends of ANS fluorescence as a function of the anionic peptide % may suggest that the solubilization role of cat-FK in excess, is preferred for the system regardless of the peptide's ability to adopt a β-sheet structure. The interaction of the scrambled version of the peptides can shed light on the mode of action of unoredered charged components like other electrolyte polymers.

In order to assess the secondary structures of the 0.3 mM PM coassemblies, circular dichroism (CD) spectroscopy data were acquired. The pure An-FD and Cat-FK solutions (Figure 1C, red and blue spectra, respectively) show low intensity spectra in which Cat-FK appears with a minimum at ~203 nm and maximum at 218 nm and An-FD seems to also exhibit these features but possibly with a contribution from an additional structural feature. Previous studies demonstrated the CD spectra of polyproline exhibits a large negative peak at 206 nm, and a weak maximum at 228 nm[72,73]. As both peptides contain Pro termini, we aimed at exploring the possibility that the spectra are showing a polyproline II (PPII) conformation. Molecular dynamics simulations (see Supporting Information, Figure S3) of Cat-FK in dilute aqueous solution provided supporting evidence for this assumption following a 100 ns simulation at which the secondary structure, as calculated using DSSP, exhibited predominantly PPII conformations, whereas Phi and Psi angles analysis suggest the coexisting of PPII and a-helix conformations. Figure 1C shows that the PM exhibit both a pronounced β-sheet contribution and the predominantly PPII conformations that was observed for the pure peptides, indicated by the ellipticity minima at 215-218 and 203 nm, respectively. To estimate the apparent tendency of

An-FD and Cat-FK PM to coassemble in β-sheet structure versus the predominantly PPII conformations, the ratio between the ellipticities, at their corresponding minima, were calculated (θ_{218} nm/ θ_{203} nm, Figure 1D, see Figure S4 raw spectra), as a function of the An-FD %. The highest β-sheet to the predominantly PPII conformations ratio appeared in this analysis for the 40-50 % An-FD composition. To assess whether the maxima in β-sheet content of this PM was a result of the two peptides coassemblies, or a result of each peptide's organization in β-sheets, we examined the CD spectra of a reference PM system, composed of Sc-FD mixed with Cat-FK (Figure 1E). Yet, since PM of Sc-FD and Cat-FK at 0.3 mM could not be monitored by CD due to aggregation, the measurements were performed with 0.1 mM PM. These Sc-FD PM showed weak CD signal that resemble the predominantly PPII conformations, according to the minima at 203 nm (Figure 1E). This result indicates that at 0.1 mM PM the Cat-FK solely cannot form β-sheet structures, by a mere screening effect of the anionic Sc-FD peptide. On the contrary, the opposite control-experiment, in which a scrambled version of Cat-FK, Sc-FK, was mixed with An-FD (Figure 1F), showed an increase in β-sheet content as a function of the An-FD percentage (Figure 1E, inset) suggesting that Sc-FK (similarly to Cat-FK) may act as a screening agent for β-sheets structures formed by a majority of An-FD. In general, the lower ellipticity observed for the Cat-FK:An-FD PM, in comparison to the Sc-FK:An-FD, is most probably a result of large coassembled aggregates that precipitate out of the solution (in accordance with the detected turbidity, Figure 1B inset), and do not contribute to the CD signal.

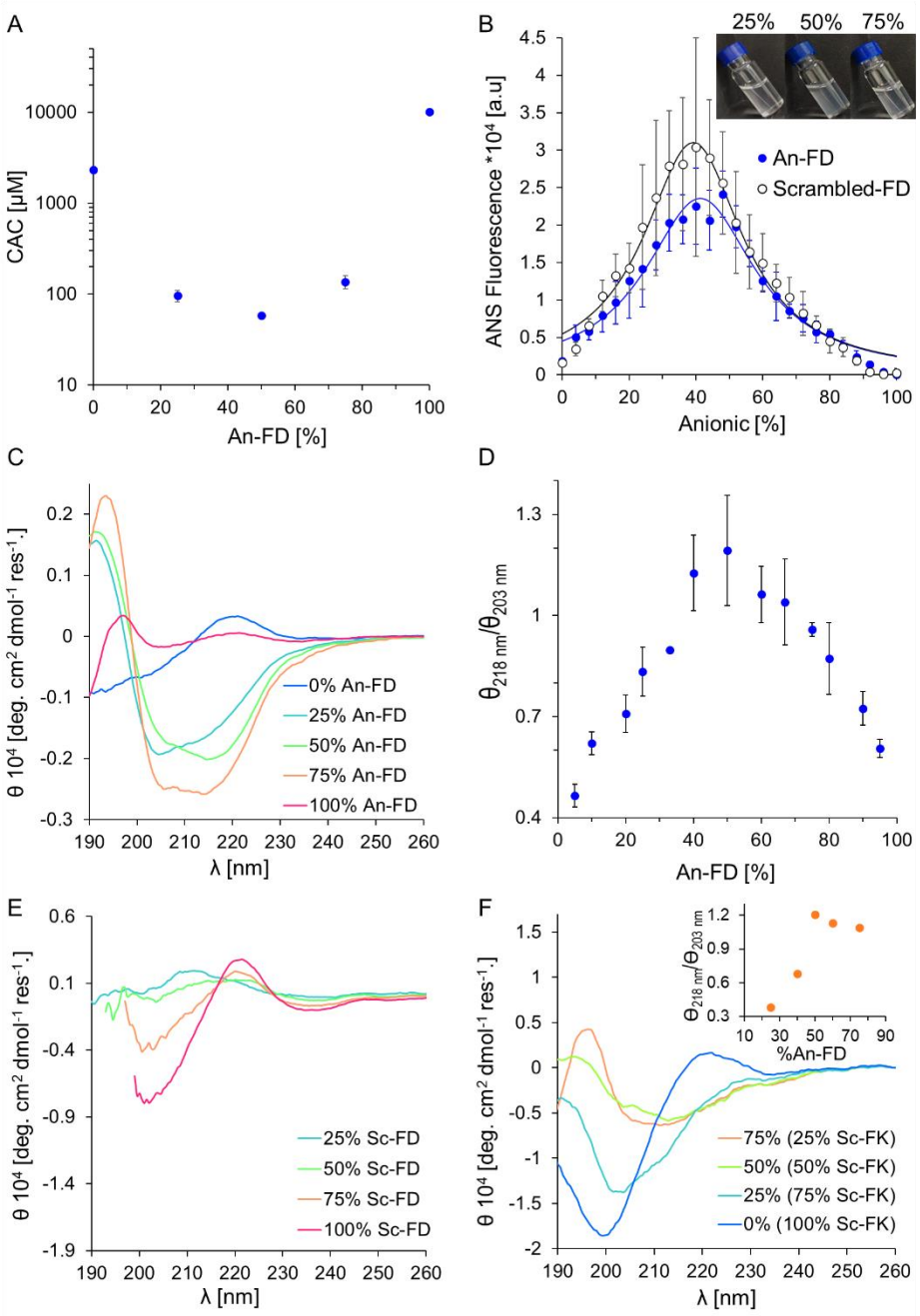

Figure 1. PM coassemblies in HEPES pH = 7.4 solutions. A. Critical Assembly Concentration (CAC) of the PM as function of the An-FD %, measured by ANS fluorescence (see also Figure S1). Mixtures were prepared by mixing the solutions of each peptide in its unassembled state, at concentrations ranging from 1 μM to 1 mM, at different volumetric ratios followed by the addition of ANS and then subjected to fluorescence measurements. **B**. ANS fluorescence of 0.3 mM PM, as a function of An-FD or Sc-FD %. Data (dots) were fitted to a Lorentzian function (lines) indicating the maximal signal is at 40 % ratio of both these anionic peptides. Inset shows

representative pictures of the PM solutions showing mild turbidity. **C.** CD spectra showing normalized ellipticity versus wavelength, of 0.3 mM Cat-FK, An-FD, and their PM at selected An-FD %. **D.** Ratio of β-sheet ellipticity minimum (218 nm) to that of the mixed conformations phase (203 nm) as a function of An-FD % for different PM and the pure peptides. **E.** CD spectra of PM composed of Sc-FD and Cat-FK at a total peptide concentration of 0.1 mM since higher concentrations could not be measured due to excessive aggregation and turbidity that is affecting the spectra at the shorter wavelengths. **F.** CD spectra of 0.3 mM PM of Sc-FK and An-FD, showing increased β-sheet content up to the 50 % An-FD, see inset representing ratio of ellipticities as in D. In B. and D. values represent an average ± SD, n = 3.

Coassemblies of fluorescently labeled An-FD and Cat-FK peptides were then visualized by fluorescence microscopy. First, each peptide solution was prepared at a concentration of 0.1 mM in HEPES 50 mM buffer at pH 7.4 (with 1 % mol/mol of the labeled peptide). Next, these solutions were mixed to form 0.1 mM PM with 25, 50 and 75 % An-FD. Figure 2 shows aggregates of the two peptides as observed by the fluorescence microscopy with images of FITC labeled Cat-FK (green color), Rhodamine-red labelled An-FD (red color) and merged images in which a yellow color indicates colocalization. Aggregates in the PM of the 25 and 50 % An-FD are ~ 10 μm in size, with the latter mixture showing also coassembled fibrils, and the 75 % An-FD shows larger clusters. This trend in aggregates size is in accordance with better dissolution, i.e., smaller aggregates, in PM with excess of Cat-FK compared to An-FD.

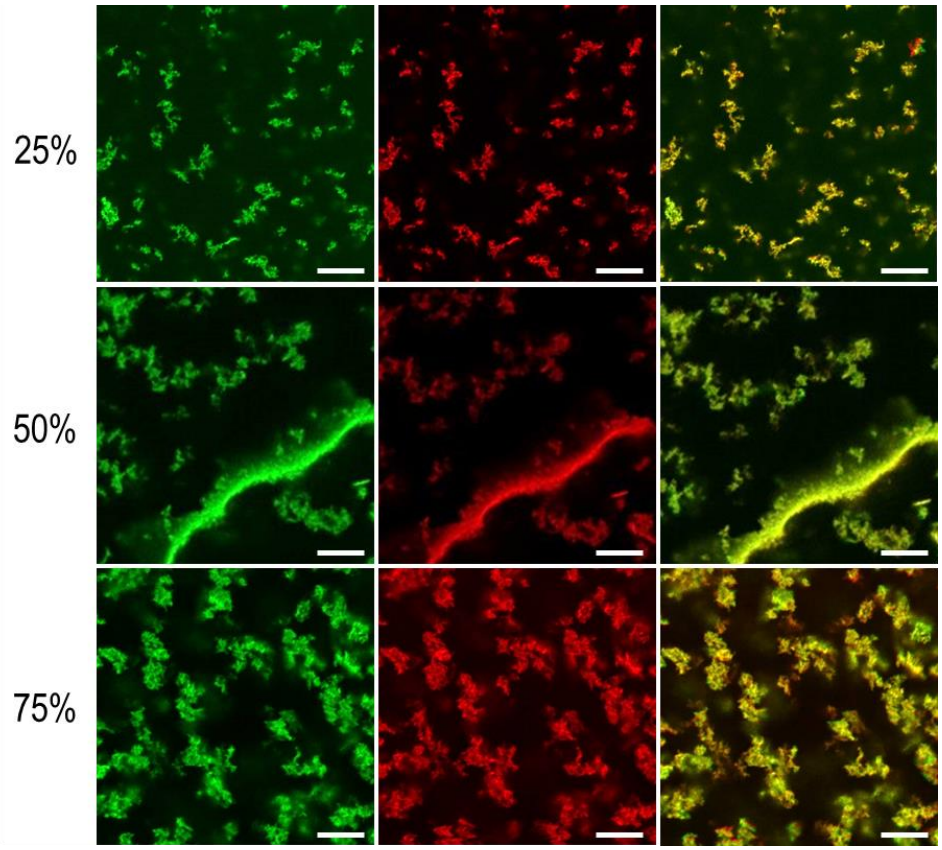

Figure 2. Fluorescently labeled PM coassemblies formed at a total concentration of 0.1 mM. Each row shows a certain PM, represented by the An-FD % in the mixture**.** FITC-labelled Cat-FK solution and Rhodamine-red labelled An-FD solution were mixed and incubated at a total concentration of 0.1 mM in HEPES 50 mM, pH=7.4 (each peptide contained 1% mol/mol of its covalently-labelled fluorescent version). The samples were imaged separately for the FITC fluorescence (left), Rhodamine-red fluorescence (middle) and the merged image of the same area were created using ImageJ software to demonstrate the coassembly of the two peptides (right). The bars correspond to 10 μm.

Figure 3 presents the cryogenic transmission electron microscopy (Cryo-TEM) micrographs of the pure peptides, An-FD and Cat-FK, at concentrations below and above their CAC values (Figure 3A and 3B, respectively). Below the CAC, at 0.05 mM, no structure was observed for each of the pure peptides (0 and 100 %, respectively) and the 50 % sample (PM 50% An-FD) shows a network of short fibrils' assemblies (Figure 3A, 50 %). This mixture contains heteromeric coassemblies, as appeared in MALDI-ToF analysis (Figure S5) and as evident in a

sample prepared with biotin-labeled Cat-FK to which Avidin-labeled gold nanoparticles were attached (Figure S6). Notably, below the CAC the effect of each peptide component on the morphology is not symmetrical, where PMs with excess of Cat-FK are smaller in the cluster dimensions and have only short fibrillar structures, and PM with excess of An-FD (> 50%) tend to have longer fibrils (Figure S6). Above the CAC, each of the pure peptides forms unique fibrillar structures (Figure 3B). An-FD forms micrometer long ones that are on average 7.6 ± 1.1 nm in width, and Cat-FK forms thinner, 4.4 ± 1.1 nm width fibrils that are sub-micron scale in length (resembling the assemblies reported previously for Cat-FK, dissolved in DIW, which were shown to elongate and align over a time-scale of several days)[74]. The frequencies of the fibrils' widths above the CAC was summarized in the histogram in Figure 3B. These TEM images suggest that above the CAC, the spontaneous self-assembly of each peptide occurs immediately following dissolution. These distinct morphologies of the pure peptides above the CAC point to differences in their assembly mechanism and the stability of the produced fibrillar structures.

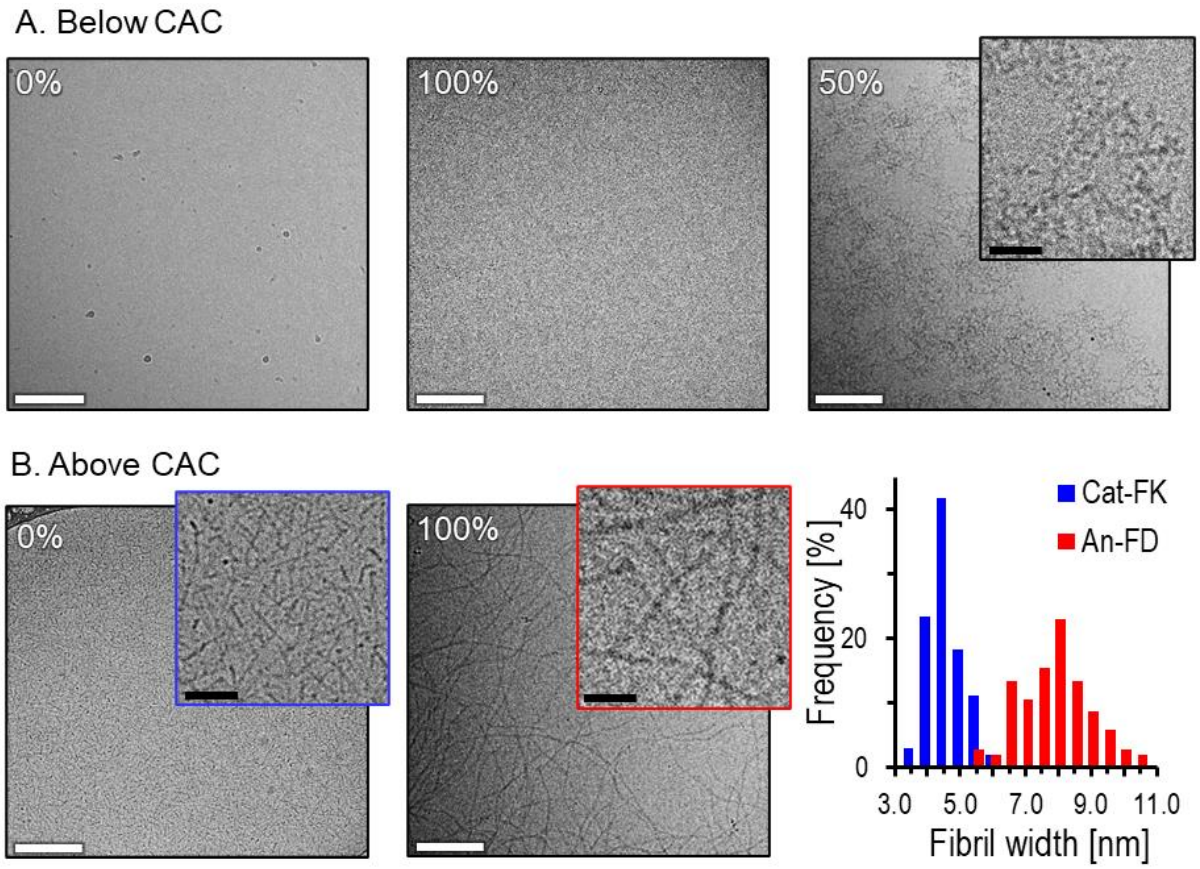

Figure 3. Cryo-TEM images of An-FD, Cat-FK and PM. A. Below the CAC, each peptide at 0.05 mM does not show notable assembly, in contrast to PM of 50% An-FD, that show nest-morphology of short entangled fibrils. Inset show a higher magnification of the 50% PM fibrils. **B.** Above the CAC, each peptide at 22.7 mM (4 % w/v) shows fibril formation. Insets show higher magnification of the fibrils. Cryo-TEM image for PM of 50 % at this total concentration could not be achieved due to excessive aggregation (Cryo-SEM analysis is shown in Figure 7). Figure on the right shows the frequency of fibrils widths above the CAC of the Cat-FK (0%) and the An-FD (100%), in which the average widths are 7.6 ± 1.1 and 4.4 ± 0.5 nm (Avg. ± SD, n = 104 and 98) for An-FD and Cat-FK, respectively. Scale bars correspond to 200 nm (white) and in inset to 50 nm (black).

To quantify the PM tendency to assemble into fibrils, the 0.3 mM mixtures were also characterized by Thioflavin T (ThT) fluorescence (Figure 4A). ThT is an indicator of β-sheet, or amyloid-like, fibrils that preferably binds to negatively-charged ones due to its cationic charge[75]. The PM showed a relatively weak ThT signal up to ~ 37 % An-FD, followed by a steep increase

of 4-folds at ~ 40 % An-FD. This step change in the ThT signal may be attributed to the PM fibrils net charge, that is positive up to the 40 % An-FD and negative for PM with higher % An-FD thus the latter may show more excessive ThT signal due to supporting electrostatic interactions. Indeed, the charge of these PM that was also monitored by ζ-potential measurements (Figure 4B), provided evidence for a net positive charge for PM with < 45 % An-FD (+16.3 mV) and a net negative charge for PM with higher % An-FD and (-6.4 mV) assuring the hypothesized charge inversion. Next, the PM were also examined with the β-sheet staining agent congo-red[76,77](CR), that unlike ThT is negatively charged at neutral pH[77] (Figure 4C). Its signal increased moderately with the increase in the anionic peptide content up to 40 % An-FD as function of the expected increase in fibrils formation and the net positive charge of these assemblies. It then showed a step increase in the CR signal, at the 40 % An-FD PM, possibly reflecting the formation of nearly equal in charge β-sheet fibrils, decorated by an excess of Cat-FK to which the CR molecules preferably bind to. In the region of PM > 40 % An-FD, the CR showed a decrease in intensity, in accordance with the formation of fewer β-sheet fibrils and its expected repulsion from the fibril's net negative charge. Based on the behavior of the two β-sheet fibrils markers, the ThT and the CR, it can be concluded that these PM fibrils are limited by An-FD in the mixtures up to 40 % and by Cat-FK at the higher % mixtures. These results corroborate the maximum hydrophobic interactions detected by the ANS for the 40 % An-FD PM. The scheme in Figure 4D summarizes the observations in which maximal β-sheet assemblies and stabilizing hydrophobic forces are found in ~40 % An-FD. Ingterestingly, this mixture exhibits increase in β-sheet structures toward nearing the stoichiometrically equality but the maxima appears at an excess of Cat-FK. The 40 % optimum in β-sheet content teaches that the excess Cat-FK, acts as an efficient solubilizing agent to the β -sheet assemblies, whereas the

An-FD is not acting similarly in this respect (note that the 60 % An-FD PM shows a significant reduction in β-sheet content in the congo red measuremtns and the supporting evidences in Figure 1). Nonethelss, the excess of each peptide contributes to the surface potential perhaps in a partially folded state. This type of interactions between folded β-sheet structure, at the core of fibrils, and unfolded ones at the periphery is common in native amyloids, known as the "fuzzy coat effect" [78–80].

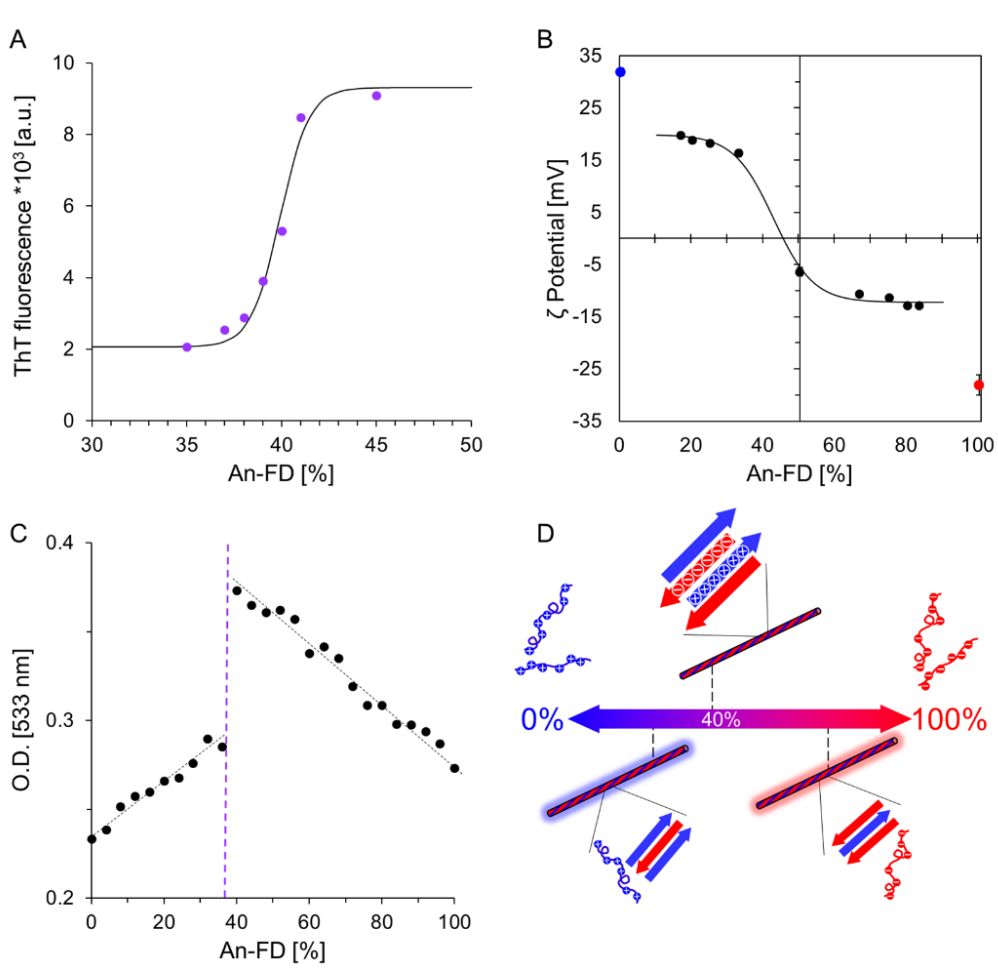

Figure 4. ThT, CR, and charge of 0.3 mM PM coassemblies. A. ThT signal (dots) fitted to a sigmoidal function (line). **B.** ζ-potentials (dots connected by a line to guide the eye). **C.** CR absorbance (dots) and lines to guide the eye. **D.** Scheme representing the fibrils formed by An-FD (red color arrow) and Cat-FK (blue color arrow) coassemblies, arranged along an arrow that highlights the fibril's charge. The distribution of both peptides within the PM was asseseed by MALDI-ToF that also supports the presence of heteromeric oligomers (see Figure S5).

Effect of pH on PMs coassembly in solution

Figure 5A shows the formal charge of the PMs, as calculated using Protein Calculator (version 3.4[81]), according to the amino acid sequence of each peptide, taking into account all residues and their relative molar ratio while ignoring possible pKa shifts due to assembly[15,63,82,83]. For An-FD the pKa of the C-terminal Pro and the side chains of Asp residues are ~3.16 and ~3.43, respectively, and the pKa of the amine deprotonation of N-terminal Pro and Lys side chains are ~7.64 and ~10.68 respectively[84]. Hence the pH range in which the two peptides can interact by complementary electrostatic interactions may extend from ~3.5 to ~10.5. For the 50 % An-FD PM the nearly zero charge range (see bold line Figure 5A) is relatively wide 5 < pH < 9.

CD spectra of 0.3 mM 50 % An-FD PM as a function of pH, was measured to assess the influence of the peptides' net-charged on their assemblies' structures (Figure 5B). The PM show a combined β-sheet and PPII structure with differences in the overall intensity as a function of the pH of the solutions. At pH = 2, the PM showed PPII structure with a minimum at 203-205 nm and a shoulder at 215 nm indicative of β-sheet forms. At pH = 3 a major effect on the spectrum intensity is noted, suggesting that the sample contains insoluble forms. Further increase to the zwitterion range, where the two peptides exhibit their fully charged state (pH = 5 - 9) resulted in increased signals of β-sheet content compared to the PPII (see the ratio of β-sheet to PPII, θ_{218} nm/ θ_{203} nm, Figure 5B). At this range where both peptides are in their fully charged state, maximal electrostatic attractions stabilize the zwitterionic mixture. Thus, not only electrostatic equivalence appears in these conditions, but also induction of the β-sheet conformation that might even induce synergistic seeding of the two peptides. This result was confirmed also using FTIR spectroscopy (Figure S7), considering the lyophilization of the sample prior to FTIR measurement that may enhance the tendency to form ordered structure such as β-sheet (special

caution was taken to minimize this effect using snap freezing in liquid-nitrogen and lyophilization at -30 ºC).When uncharged, both peptides may adopt β-sheet conformation due to their intrinsic amphiphilic sequence[3,15], while in their charged state the repulsion between their own side chains induces maximal distance between these residues and a resultant PPII conformation. Hence, outside of the zwitterionic range (pH < 3 or pH > 9) only one peptide component is charged while the other is uncharged. Under these conditions it can be expected that the uncharged peptide will undergo self-assembly while the other charged peptide will remain soluble in solution. The results indeed indicate that at pH = 2 and 3 An-FD is folded into β-sheet while Cat-FK is probably responsible for the PPII signal. The opposite occurs at pH = 11, where Lys side chains are uncharged and Cat-FK is organized in β-sheets whereas An-FD is charged and soluble.

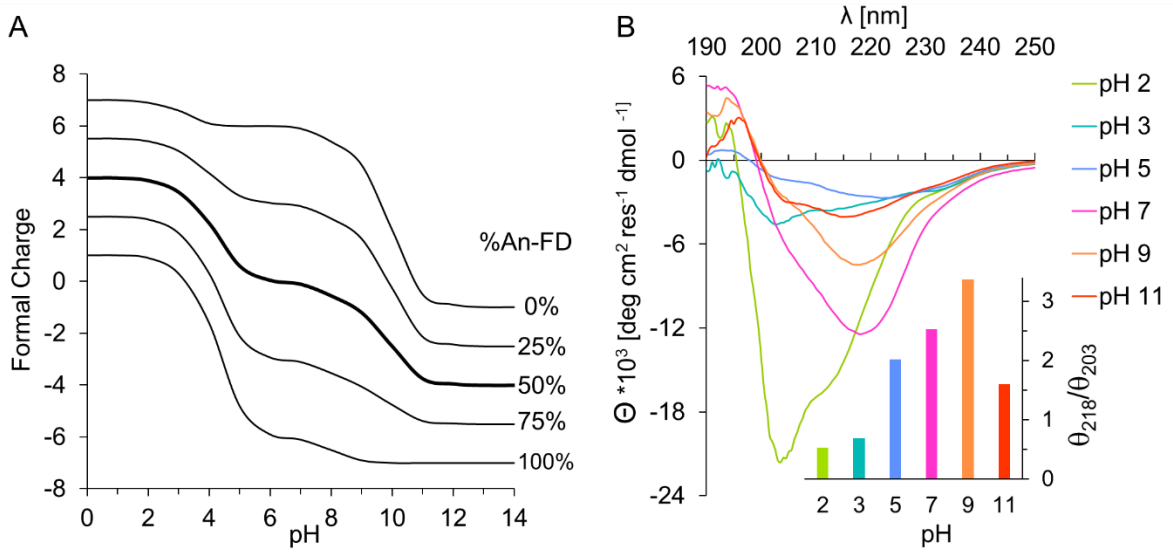

Figure 5. The effect of pH on PM structures. A. Calculated formal charge of the PM as function of the pH considering the amino acids in the sequence (the bold line of 50 % An-FD refers to the samples of part B). **B.** CD spectroscopy of 50 % An-FD (molar ratio of 1:1 An-FD:Cat-FK) at different pH values showing a combination of β-sheet and PPII structures (see inset). In addition, secondary structure analysis of the PM which was performed by Fourier Transform Infrared Spectroscopy (FTIR) showed amide-I vibration typical to antiparallel β-sheet structure (Figure S7).

Figure 6A shows the Isothermal Titration Calorimetry (ITC) curves produced by titrating Cat-FK to either An-FD or Sc-FD. Titration of Cat-FK to An-FD produced a dominant exothermal interaction with positive values starting from ~7 μJ and decreasing after saturation to the blank value (~ 0.4 μJ). This pattern is typical to a single mode interaction[85], which is associated with the electrostatic complementary interactions between the Lys and Asp resides of the two peptides. The titration of Cat-FK to Sc-FD (Figure 6A, turquoise curve) showed an endothermal, negative values, at the beginning of the measurement which becomes weakly exothermal, after nine injections, at close to the equimolar ratio between the peptides. Figure 6B shows the fitting of the heat pattern of Cat-FK titrated into An-FD in Figure 6A, to unspecific single-type interactions' model between the two components, that results in a high coupling enthalpy (ΔH = -35 kJ mol^{-1}), with n = 1.12 corresponding to close to equimolar interactions, with a small excess of Cat-FK over an-FD in accordance with the excess of the cationic peptide in the maximally detected hydrophobic assemblies by ANS and fibrillar assemblies detected by ThT and CR (see Figure 1B and Figure 4A and 4C, respectively). The Gibbs free energy was calculated to be ΔG = -36.65 kJ mol^{-1} with an entropy change of ΔS = 5.871J mol^{-1} K, assuring that this complexation is spontaneous. The enthalpy is expected to be negative thanks to the cross-strand β-sheet hydrogen bonds and the interactions between the electrostatically complementary peptides. The positive entropy could be associated with the release of counter ions from each of the peptides upon the formation of the charge-complementary interactions. Based on the data analysis, the dissociation constant, K_d, for Cat-FK:An-FD complexes was determined to be ~ 40 μM, with a confidence interval in the same range. An additional analysis of the dissociation constant that was performed by microscale thermophoresis (MST) revealed value in the same order of

magnitude (50 ± 8 µM, Figure S8). In comparison, the titration of Cat-FK to Sc-FD by ITC resulted in a positive enthalpy value, $\Delta H = 6 \pm 12$ kJ mol^{-1} with a ΔG = -35.39 kJ/mole and ΔS = 138.9 J mol^{-1} K^{-1}. Interestingly, both coupling of Cat-FK with either An-FD or Sc-FD is favorable as indicated by the negative Gibbs free energy values. Yet, while for An-FD the interaction is primarily enthalpy-driven, for Sc-FD it is entropy-driven. The binding of Cat-FK to Sc-FD apparently does not yield an overall favorable intermolecular interactions contribution, but rather an increase in entropy due to probable release of counterions from each of the peptides following their complexation. Likewise, similar processes were detected using ITC in systems of polyelectrolyte complexes, where complexation and release of ions were competing processes[86,87].

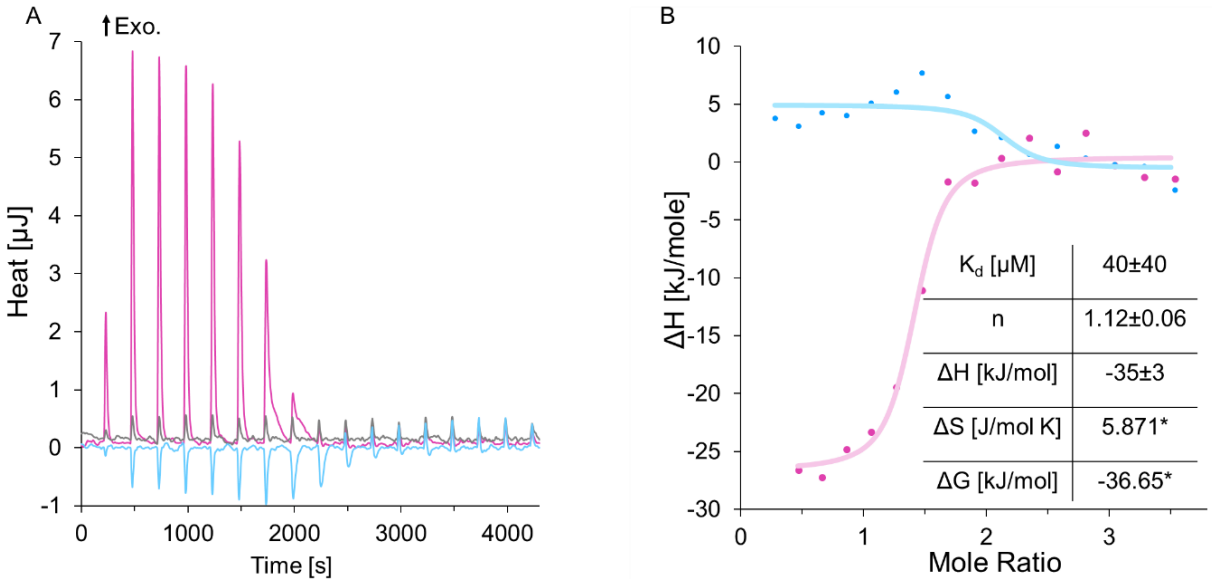

Figure 6. ITC measurements of Cat-FK titrated into An-FD. A. Titration of Cat-FK into An-FD (pink), Sc-FD (turquoise) solutions and to a buffer (grey). **B.** Enthalpy versus mole-ratio (dots) with a fit to unspecific single-type interactions' model (colour scheme as in A). Table inset shows the parameters fitted to Cat-FK titrated into An-FD. Data was fitted using NanoAnalyze software, to the independent model ± confidence interval. *The entropy and free energy values are derived from the fitted model rather than from the collected points.

PM prepared from stock peptide solutions at above CAC

PM prepared from stock solutions of the peptides at above their individual CAC values, 22.7 mM (4 % w/v), generated in some cases a hydrogel phase. Figure 7A shows the vials containing 100 µL of the 4 % w/v PM. The vials positioned in upside down orientation (poor man rheology) demonstrate for the hydrogels the self-supporting solid like appearance[88]. Pure An-FD and the 5 % An-FD PM did not form a hydrogel phase whereas the PM with 8 to 33 % An-FD stabilized hydrogel phases. At higher An-FD percentages the PM formed viscous and turbid solutions. Furthermore, turbidity was apparent in all PM with > 13 % An-FD with a noticeable maximal aggregation at 50 % An-FD. Figure 7B shows the cryogenic scanning electron microscopy (Cryo-SEM) images of the 5 and 50% PM solutions and the 33 % PM hydrogels, all presented with dense fibrillar morphologies, confirming that fibrillar assemblies are present in both the solution and hydrogel phase samples. The hydrogels of PM with 25-35 % An-FD were also characterized by rheological measurements that showed soft viscoelastic behavior with G' greater than G", with the 35 % An-FD exhibiting the highest values (Figure S9).

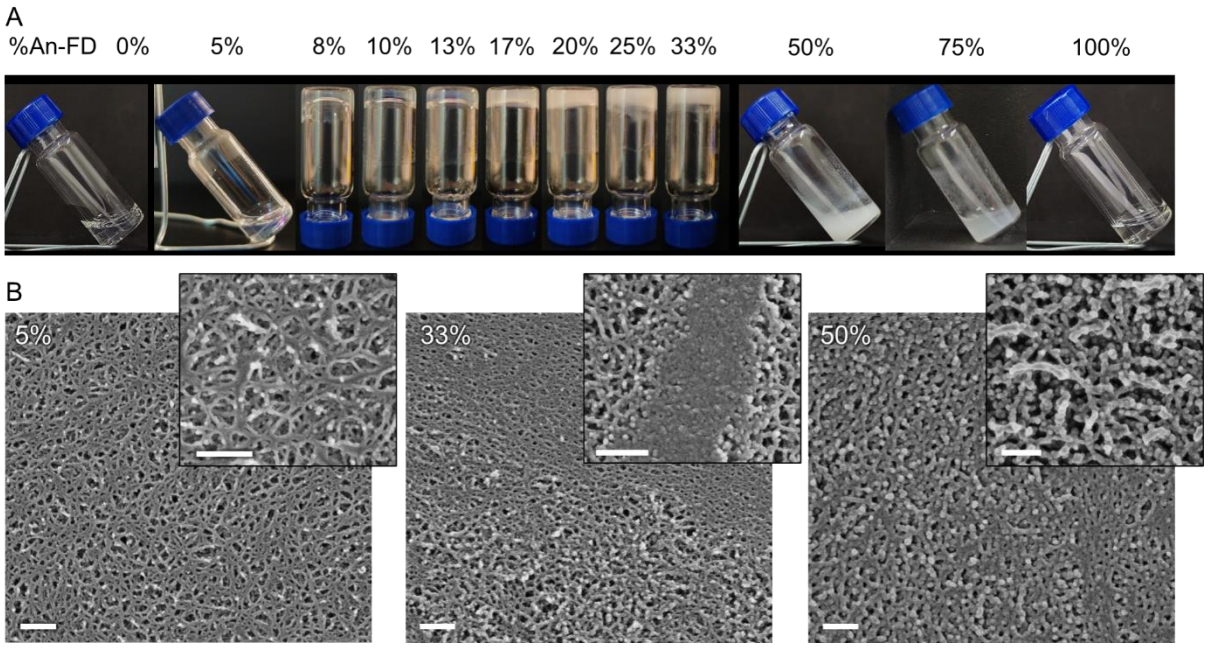

Figure 7. PM above the 4 % w/v CAC. A. Vials with PM at different % An-FD with such turned upside down to demonstrate hydrogel formation. **B.** Cryo-SEM images of hydrogel (33 %) and PM solutions (50 and 5 % An-FD); Bar corresponding to 200 nm.

SAXS and XRD of PM below and above CAC

The pure peptides and the PM prepared at above CAC concentration, 4 % w/v (22.7 mM) were characterized by SAXS (in soluble and hydrogel states), and XRD (following lyophilization at -30 ºC). The XRD of the different An-FD % PM (Figure 8A) revealed Bragg peaks corresponding to the repeat distances 23, 11.6, 5.8, and 4.8 Å. SAXS of the same PM measured in their solution state, showed a 46 Å spacing, in addition to the 23 and ~12 Å spacing (Figure 8B). All these peaks can be associated with a unit cell of a = 9.6 , b = 46 Å (and a c axis which corresponds to the thickness of the well-known peptide bilayer packing, Figure 8C[74]). The XRD peak at 4.8 Å which was observed for all PMs and the pure peptides, is typical for the hydrogen bond spacing within the β-sheet structure[89,90]. The 46 Å spacing observed by SAXS corresponds to the axial length of both An-FD and Cat-FK peptides in the β-sheet conformation (the distance between Cα atoms along a peptide in β-sheet conformation is 3.45 Å, hence, a 13 amino acids peptide extends to ~ 45 Å)[65,74] The unit cell which is presented in

Figure 8C, may accommodate each of the peptides and their mixtures, comprises of four molecules, two of which are related by the common antiparallel β-sheet arrangement and linked by inter-strand hydrogen bonds (defining the *a* axis). The fibril bilayer exhibits a two-fold-like symmetry along the *c* axis whereby the hydrophobic Phe side chains, from each layer point at each other to create a hydrophobic core. In this low-resolution X-ray scattering measurements, the 11.6 and 12 Å peaks may correspond both to a higher order of the 46 Å peak noted as (0,4,0), and to the thickness of one peptide layer in laminated bilayer fibrils as noticed in SAXS measurements above the CAC (Figure 8B). Of note, the XRD patterns suggest enhanced crystallinity of the PM systems compared to the pure peptides evident by the enhanced intensity of the XRD peaks. Similar peaks to those detected above, appeared also in PM formed at concentrations below the CAC of the parent peptides (Figure S10), suggesting that even below CAC fibrils may exist or that in the lyophilization process coassembly of the two peptides into fibrils with same unit cell may occur.

Furthermore, the SAXS curves of the different PM above the CAC (Figure 8B) provide additional information on the different assemblies in solution and hydrogel phase. Cat-FK solution shows a moderate slope at low q values, representing assemblies with a finite sub-micron size, as was previously reported[74]. The SAXS curve of An-FD solution corresponds to long one-dimensional assemblies (in which the limiting slope of the intensity is $I(q) \sim q^{-1}$). These findings could support a model in which short fibrils of Cat-FK (as detected by cryo-TEM, Figure 3 above) stabilize long fibrils of An-FD (illustrated schematically in Figure 8C,D).

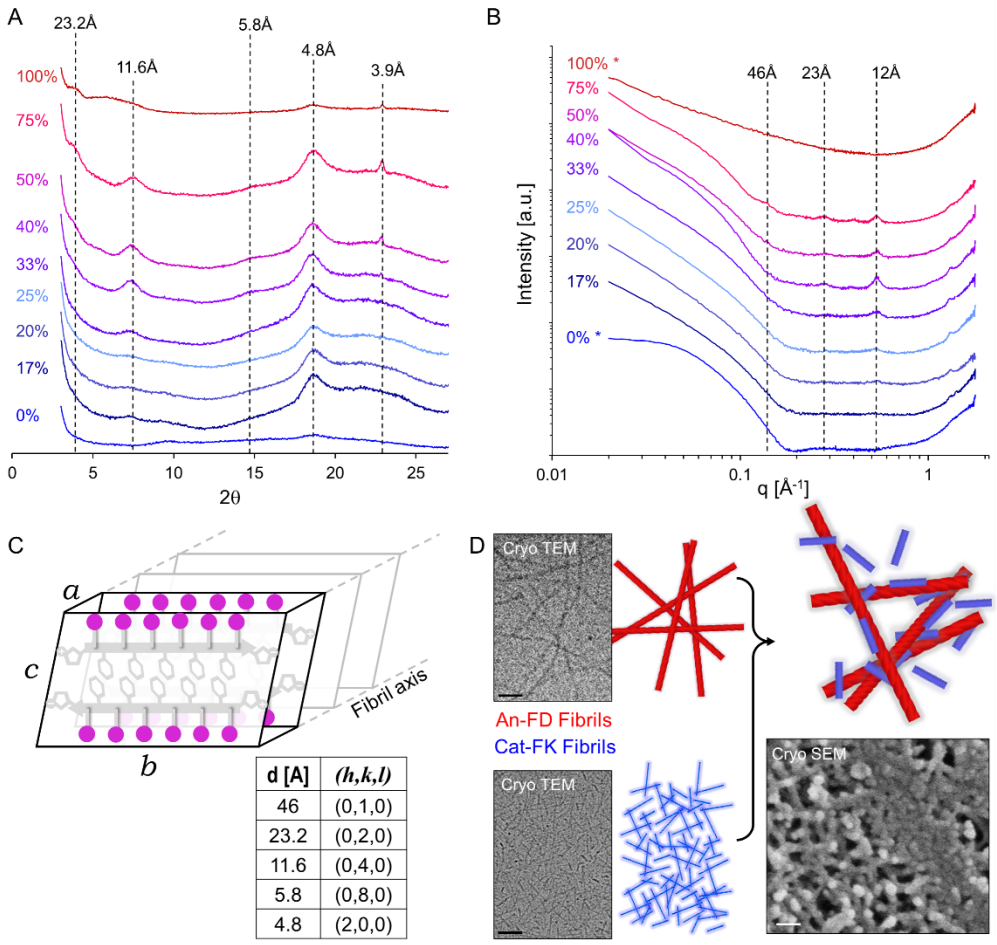

Figure 8. Structural analysis of PM by XRD and SAXS. A. XRD pattern of lyophilized An-FD, Cat-FK and their PM, at a total concentration above the CAC, 22.7 mM, **B.** SAXS of these pure peptides and PM at 22.7 mM (above CAC). **C.** A scheme of the proposed unit cell comprising the fibrils; inset Table assigning the detected repeat distances to Miller indices. **D.** A scheme of the PM fibrils above the CAC (including cryo-TEM images from Figure 3, of the pure peptides at 22.7 mM, and cryo-SEM image of 33% An-FD gel; bar corresponds to 50 nm).

Conclusions

The results of this study can be summarized in the scheme shown in Figure 9. Upon mixing solutions of each peptide below its CAC concentration, these unfolded peptides in the PM system may undergo a cooperative coassembly process and form β-sheets with each other (Figure 9, right side).

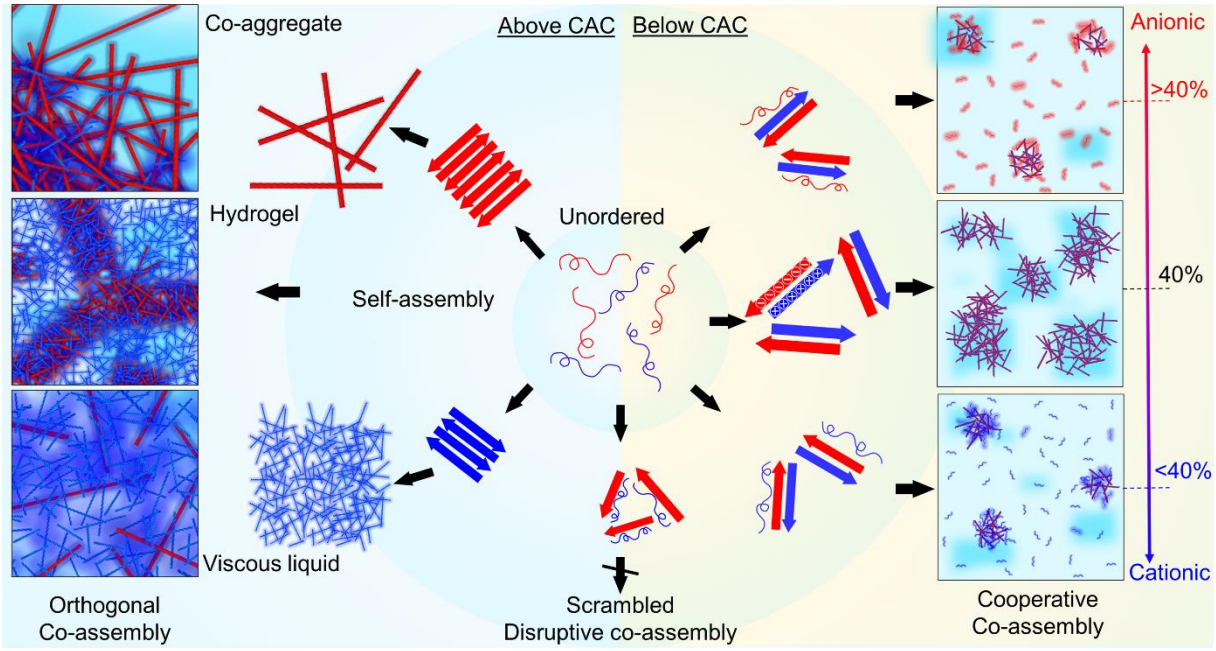

Figure 9. The main pathways in coassembly of the charged β-sheet forming peptides Cat-FK and An-FD. ***Below the CAC*** (right side of the scheme) the unordered peptides can undergo cooperative heteromeric coassembly, particularly including hydrophobic interactions and formation of β-sheet (seen in Figure 1 and Figure S3-4). Maximal assembly to β-sheet is achieved in contribution of both peptides (Figure S4, S6), while excess of either of them can influence the surface charge of the fibril and dominate the outer layer of the assembly (Figures 4 and Figure S5). Incorporation of scrambled sequence leads to binding entropically-driven disruptive coassembly, avoiding the fold into precise ordered structure (down arrow, based on Figures 1,6 and Figure S5). ***Above the CAC*** (left side of the scheme) the peptides first undergo homomeric *self*-assembly (based on Figure 1,3 and 8) which is followed by their orthogonal coassembly into either viscous solution or a hydrogel phase (as seen in Figure 7-8 and Figure S9).

Previous studies indicated that system lacking charges, either due to the peptide concentrations or the amount of charged residues, tend to allow "self-association" rather than co-association,

leading to combinations of coassembled oligomers and homogeneous self-assembled ones[53,54]. Yet, higher charge systems tend to favor co-association of multicomponent oligomers, leading to cooperative assemblies. Echoing these observations, here we demonstrate these two types of coassemblies; Up to the 40 % An-FD there is an increase in the formation of hydrophobic niches of coassemblies that bind ANS and form β-sheets as evident by CD. The β-sheets may also coassemble into small fibrils (Figure 2 and 4) that are detected by ThT and CR markers. The 40 % An-FD appears to be the sweet point of β-sheet-fibrils formation, whereby the small excess of Cat-FK is possibly used by the system, to decorate the assemblies and enhances their solubilization. Interestingly, the CD measurements indicated a maximum of β-sheet formation at 50 % An-FD suggesting that the PM solution holds various forms of β-sheet coassemblies, that are possibly undetected by ANS nor by ThT and CR. These different experimental assays may be utilized in future studies to reveal the detailed kinetic mechanism of formation of these soluble PM coassemblies.

Upon mixing of stock solutions, of each peptide at above its CAC, a coassembly did occur which led to either precipitation or to hydrogel formation (Figure 9, left). Our observations indicate that hydrogel phase is formed when PM enabled coassembly with excess of the cationic peptide. These hydrogels probably consist of An-FD long fibrils that are physically crosslinked by short Cat-FK fibrils. On the contrary, excess of An-FD relative to Cat-FK results in insoluble macroscopic aggregates that are formed probably by An-FD intermingled with Cat-FK. These experimental results underscore the elusive optimum point for maximizing coassembled structures by electrostatic interactions; neither maximal assembly, folding or the strongest interaction between the components can guarantee specific physical characteristics, as the

cooperation between the components should be experimentally verified to reveal the various soluble and insoluble assembly forms.

Experimental

Materials:

The peptides Pro-Asp-(Phe-Asp)$_5$-Pro, An-FD (Mw of 1638.65), Rhodamine-red N-terminal-labeled An-FD, Rhod-FD (Mw = 2063.47), Asp-Phe-Phe-Pro-Asp-Asp-Pro-Phe-Asp-Phe-Phe-Asp-Asp, Sc-FD (a scrambled version of An-FD), Pro-Lys-(Phe-Lys)$_5$-Pro, Cat-FK (Mw of 1717.16), FITC N-terminal-labeled Cat-FK, FITC-FK (Mw = 2219.72) and Lys-Phe-Phe- Pro-Lys-Lys-Pro-Phe-Lys-Phe-Phe-Lys-Lys, Sc-FK (a scrambled version of Cat-FK) were all custom synthesized, purified by high performance liquid chromatography to >95% and supplied as lyophilized powders (An-FD by American Peptide, Sunnyvale, CA, Rhod-FD by Caslo, Lyngby, Denmark and Cat-FK by GenScript, Piscataway, NJ). Peptide content was adjusted following removal of the residual anions trifluoracetic acid (TFA), acetic acid and hydrochloric acid by ion exchange chromatography to 77.7 % for Cat-FK and 92.0 % for An-FD. Briefly, peptides aqueous solutions at 1, 0.1 and 0.01 mg/mL concentration were injected (500 µL) into an anion exchange column (Dionex IonPAc^{TM} AS9-SC, 4x250 mm) that ran continuously with 2 ml/min of the isocratic solution 2 mM Na_2CO_3 and 0.75 mM $NaHCO_3$. Concentrations were calibrated using reference solutions containing the three ions prepared by dissolving glacial acetic acid, TFA and hydrochloric acid (%) in DIW and serial dilution thereof.

Hydrochloric acid (35%), sodium hydroxide (99%), 8-Anilino-1-naphthalenesulfonic acid (ANS), Thioflavin T (ThT), Congo-Red (CR) were purchased from Sigma-Aldrich (Rehovot, Israel). Au-streptavidin nanoparticles, 10 nm colloidal suspension in tris buffered glycerol

aqueous solution ($OD_{520\ nm}$ = 2.5) was purchased from Sigma-Aldrich (LOT #SLCB9629). HEPES buffer powder (Mw of 238.3) was purchased from Holland-Moran (Yehud, Israel).

***Peptide solutions*:**

Peptide solutions, at concentrations of 0.05-22.7 mM (~0.009 - 4% w/v), were prepared by dissolving lyophilized peptide powders in deionized water (DIW, 18.2 MΩ cm, Thermo Scientific) followed by the addition of concentrated HEPES buffer (1M stock solution, pH=7.4) to a final buffer concentration of 50 mM. Next, solutions were sonicated for 30 seconds by a probe-sonicator operated at 40 % amplitude (Sonics Vibra-cell VCX-130, Newtown, CT, USA), to accelerate dissolution and assure the homogeneity of the sample. The peptide solutions were then diluted to the required actual concentration, while taking the peptide purity and content into account, using the same buffer (HEPES 50 mM, pH=7.4). Following the dilution, the pH was measured and corrected when necessary, using aliquots of 5 M or 1 M NaOH or HCl aqueous solutions. Peptide samples were then vortexed in the desired ratio of An-FD to Cat-FK. For example, 0.3 mM sample of 75% An-FD is prepared by mixing different 3:1 v/v An-FD:Cat-FK, of each of the peptides' 0.3 mM solution.

For the pH-dependent measurements, the peptides were dissolved as described above in DIW (70% of the total volume), samples were titrated with NaOH and HCl (5M, 1M and 0.1M solutions) to the desired pH and then diluted with DIW to the final volume. Last, the samples were sonicated, and the pH was measured and corrected again if necessary (allowed deviation of < 0.1 pH unit). PM at different pH values were prepared by adjusting the pH of each peptide solution followed by their mixing together.

Confocal fluorescent microscopy

FITC-labelled Cat-FK and Rhodamine-red labelled An-FD were co-incubated in PM at concentration of 0.1 mM (HEPEs 50 mM, pH=7.4). The content of fluorescently labelled peptides was 1% (molar ratio) in both An-FD and Cat-FK separate solutions prior mixing. The PM were prepared as described above and let incubate at RT for one-hour prior imaging, and placed on confocal dish (Nest, China). The samples were imaged on high resolution confocal fluorescence microscopy (LSM880 Axio-Observer Z1 microscope, Zeiss, Germany, equipped with Z-Piezo Stage Controller). The samples were imaged separately for FITC fluorescence, Rhodamine red fluorescence and the merged picture of the same area was created using ImageJ software to estimate the co-localization of the two peptides.

ANS fluorescence

Peptide mixtures were prepared as described above in 50 mM HEPES buffer solution. ANS is a useful label of unspecific hydrophobic proteinaceous aggregates formed through liquid-liquid phase separation (LLPS)[91,92], a process that is taking place at early stages of assembly in solution[93]. A solution of ammonium 1-anilino-8-naphthalene sulfonate (ANS) was prepared with 1 mg ANS in 50 mL DIW (equal to 63.2 μM). This stock solution was kept protected from light at room temperature (RT). The peptide/ANS samples were equilibrated at RT for one hour. Next, 54 μL of peptide solution (either mixture or one peptide, in concentration of 0.3 mM) were mixed with 6 μL of the ANS solution (final ANS concentration of 6.3 μM) and the samples were incubated for two hours prior measurement. The samples were placed in 384-well black plate (Greiner bio-one) with each 60 μL per well, in three technical replicas. The fluorescence was measured on Biotek Synergy H1 plate reader (Biotek, Winooski, VT, USA) at 25 °C (λ_{EX} = 350 nm, λ_{EM} = 500 nm)[91]. The error bars represent three independent PM samples that were measured at the same time.

Circular Dichroism (CD) Spectroscopy

CD spectra were recorded in a range of 190-260 nm on a Jasco J-715 spectropolarimeter (Tokyo, Japan), with 0.01 cm quartz cuvettes. All samples were prepared in diluted 5 mM HEPES buffer to minimize CD background noise. Spectra were recorded at a final PM concentration of 0.3 mM. PMs at different pH values were prepared at 0.4 mM titrated with NaOH 0.1M and 5 M or HCl 0.1 M and 5 M to the desired pH, then further diluted with DIW to the final concentration of 0.3 mM. CD spectra were recorded at 0.5 nm wavelength data pitch at 25 °C and represented as an average of four scans. CD signals of the buffer were recorded and subtracted as background from the corresponding spectra. The CD scans are presented in mean reside ellipticity as function of wavelength. Further analysis presents the ratio between the mean residue ellipticity minima of the β-sheet at 218 nm to that of polyproline type II at 205 nm.

Measurement of the Critical Aggregation Concentration (CAC)

Peptide samples were prepared as described above in final peptide concentration of 22.7 mM in HEPES 50 mM, pH 7.4. Then, the samples were serially diluted in Eppendorf tubes by transferring 400 µL of peptide solution, complemented by 200 µL for 15 times. The samples were then sonicated in a bath sonicator for 10 minutes. Samples were placed in 384 well black plate, 54 µL in each well with three technical replicas and each well was supplemented with 6 µL of the ANS solution (described above). The samples were protected from light, incubated at RT for two hours and then the ANS fluorescence was measured as described above. The fluorescence was analyzed as a function of the total peptide concentration. The CAC was determined as the point at which the slope of the fluorescence increases by one order of

magnitude from the intercept of two linear trends of the fluorescence, at low and high concentrations[91].

Congo Red (CR) labeling

Similar peptide mixtures that were prepared for ANS fluorescence assay were also labeled with Congo Red (CR) as fibril labeling agent[94]. A solution of CR 10 mM in DIW was prepared and used as a stock solution. Prior to each experiment the solution was diluted with HEPES 50 mM buffer to final CR concentration of 100 μM. Peptide samples of 54 μL (either PMs or each peptide, at a total concentration of 0.3 mM) were mixed with 6 μL of the CR solution (final CR concentration of 10 μM). The samples were incubated for ten minutes, and then placed in 384-well flat bottom clear plate (Greiner bio-one). Each well was filled with 60 μL of the peptide/CR sample, and measurements were carried with three technical replicas. Optical absorption (OD) of CR was collected between 400-600 nm on a plate reader (Multiskan GO, Thermo scientific, Waltham, MA). The CR-fibril-related OD maxima was found to be at 533 nm and that was used as a measure of fibril assembly.

Thioflavin T (ThT) Fluorescent labeling

Peptide coassemblies were prepared in solution as described above, in total peptide concentration of 0.3 mM at the desired peptide ratio, all in HEPES buffer (pH=7.4, 50 mM). The samples were let to stabilize for one hour at RT. Then, three technical replicas of 54 μL of each sample were placed in 384-well flat bottom black plates (Greiner Bio-one), supplemented with Thioflavin T (ThT), 6 μL, 10 μM (from stock aqueous solution of 100 μM) and complemented to a final volume of 60 μL. The samples were shaken for 10 seconds. ThT fluorescence from the

dye supplemented peptide solution was measured on Biotek Synergy H1 plate reader (Biotek, Winooski, VT, USA) at 25 °C (λ_{EX}= 440 nm, λ_{EM} = 490 nm).

ζ-Potential

ζ potential values of peptide buffered solutions (PMs 0.3 mM) were measured by Zetasizer (Zetasizer Nano ZS, Malvern, Worcestershire, UK). The samples were allowed to stabilize for 60 seconds and then the ζ-potential was measured in DTS1080 U-type polystyrene cuvette in three separate scans, each with three technical replicas.

Formal Charge calculation

The sequences of An-FD and Cat-FK were analyzed using Proteopedia encyclopedia for biomolecules[81,95]. The formal charge of each peptide sequence was calculated at various pH values, ranging from 0 to 14 in 0.1 pH unit steps. The peptide mixtures' formal charge was then calculated as the linear combination of the formal charge of each peptide in accordance with its fraction. These calculation do not take into account assembly aspects and related pKa shifts.

Isothermal Titration Calorimetry (ITC)

Cat-FK (0.5 mM) was dissolved as reported above in HEPES buffer (pH = 7.4, 50 mM) and titrated into An-FD solution (0.05 mM in same buffer), using Nano ITC low volume cell (TA Instruments, Newcastle, DE, USA) applying 17 drops (3 µL each) after temperature stabilization to 25˚C. Following each drop the system was stabilized for 100 seconds. As a negative control, similar titration of Cat-FK was applied to Sc-FD (scrambled sequence of An-FD that does not form β-sheet structure, prepared similarly to An-FD). Titration of Cat-FK to similar buffer was

used as a baseline. The resulted isotherm was analyzed using Nanoanalyze software using an independent interaction model with model fitting of 99%.

Cryogenic Transmission Electron Microscopy (Cryo-TEM)

Peptide solutions were prepared as mentioned above (total peptide concentration 0.05 mM) in buffer. Following 30 min of incubation at room temperature, 3 μL of the sample's solution was deposited on a glow-discharged TEM grid (300 mesh Cu Lacey substrate grid; Ted Pella). The excess liquid was blotted out with a filter paper and the specimen was rapidly plunged into liquid ethane precooled with liquid nitrogen in a controlled environment (Leica EM GP). The vitrified samples were transferred to a cryo-specimen holder (Gatan 70° FOV Cryo-transfer Holder) and examined at −181 °C with a FEI Talos F200C is a 200 kV FEG Transmission Electron Microscope operated at 200 kV in low-dose mode. Images were recorded with a Ceta 16M CCD Camera.

Peptide hydrogel preparation

Hydrogels (4% w/v, 22.7 mM) were prepared by mixing of the two peptide solutions. Each peptide was dissolved in HEPES 50 mM buffer, pH=7.4, applying 30 seconds sonication using probe-sonicator at 40% amplitude (Sonics Vibra-cell VCX-130, Newtown, CT, USA) to accelerate dissolution. The peptide solutions pH was measured and corrected using 5M or 1M NaOH or HCl aqueous solutions, followed by another 30 seconds sonication to increase the peptide solution homogeneity prior to gel formation. The two peptide solutions (4% w/v, An-FD or Cat-FK) were clear to naked eye. To prepare gels, the two peptide solutions were mixed using sterile syringe, An-FD solution to Cat-FK solution within Eppendorf plastic vial, and the mixture was mixed by a vortex. The mixture was transferred into the desired vial/plate, and stabilized

overnight at 4˚C. The hydrogels were brought back to room temperature prior to further characterization or any other experiment. Not all 4% w/v PM formed gel, and in some ratios forms viscous solutions or biphasic behavior with solid sediments.

Cryogenic Scanning Electron Microscopy (Cryo-SEM)

PM gels were placed between two aluminum discs (3mm in diameter, 25μm in thick each) and cryo-immobilized in a high-pressure freezing device (EM ICE, Leica). The frozen samples were then mounted on a holder under liquid nitrogen in a specialized loading station (EM VCM, Leica) and transferred under cryogenic conditions to a sample preparation freeze fracture device (EM ACE900, Leica). In that device the samples were fractured by a rapid stroke of a cryogenically cooled knife, exposing the inner part of the sandwiched discs. After fractured, the samples were etched at −100 °C for 10 minutes to sublime ice from the sample surface and coated with 3nm carbon. Samples were imaged in a Gemini SEM (Zeiss) by a secondary electron in-lens detector while maintaining an operating temperature of -120 °C.

Small Angle X-ray Scattering (SAXS)

The 22.7 mM (4% w/v) peptide samples, either hydrogels or solutions, were prepared as described above. SAXS patterns of the solutions and hydrogels were obtained with a SAXSLAB GANESHA 300-XL. CuKα radiation was generated by a Genix 3D Cu source with an integrated monochromator, three-pinhole collimation, and a 2D Pilatus 300K detector. Hydrogel specimens were placed in stainless steel sample cells with entrance and exit windows made of mica. Solutions (of the pure peptides) were placed into a 1.5 mm quartz glass capillary (wall thickness of 0.01 mm). The scattering spectra of the solvent were subtracted from the corresponding solution data using the Irena package for analysis of small-angle scattering data. The scattering

intensity q was recorded in the range $0.02 < q < 1.4$ $Å^{-1}$ (corresponding to repeating lengths 4 – 320 Å). Measurements were performed under vacuum at ambient temperature. The scattering curves were corrected for counting time and sample absorption.

X-ray diffraction (XRD)

Powder X-ray diffraction (XRD) measurements were performed on cryogenically-freezed and lyophilized peptide powders. PMs at 22.7 mM (4% w/v) were prepared as described above but for using the buffer ammonium acetate (10 mM, pH = 7.4) expected to evaporate off the sample under lyophilization. Following overnight stabilization of the hydrogels the samples were snap frozen in liquid nitrogen and then lyophilized in temperature-controlled protocol at -30˚C to minimize structural changes along the lyophilization. The relatively low concentration of buffer (10 mM) was used to minimize the buffer-salt XRD fingerprint. X-ray diffraction measurements, θ/2θ geometry, were performed on a powder diffractometer (Empyrean, Panalytical B.V., Almelo, the Netherlands) equipped with position sensitive detector X'Celerator, using Cu Kα radiation (λ= 1.5417 A) at 40 kV and 30 mA. Scans were acquired during ~15 min in 2θ range, 2– 30°, at ~0.033° step size.

Acknowledgments

The measurements of electron microscopy, SAXS, XRD, ITC, MST, ζ-potential and rheology were performed at the Ilse Katz Institute (IKI) for Nanoscale Science and Technology Ben-Gurion University of the Negev, Beer Sheva, Israel. The authors are thankful to Dr. Einat Nativ-Roth for her great support, fruitful comments and help in sample preparation for electron microscopy, measurements and imaging of cryogenic TEM and SEM; to Dr. Alon Zilka for his assistance in MST experiment, Dr. Sofiya Kolusheva for her critical comments during ITC data

analysis, Dr. Mark Karpasas for performing the rheological measurements and Dr. Yelena Mirsky for measuring XRD. H.R. is grateful to the Avram and Stella Goldstein-Goren funds for supporting this study.

Supplemental Information

The following files are available free of charge.

AUTHOR INFORMATION

Corresponding Author

Hanna Rapaport, E-mail: Hannarap@bgu.ac.il

Author Contributions

E.A, T.L, Z.A, I.C.E and H.R designed the research; E.A. performed the ITC, MST, ζ-potential, ThT-fluorescence, CR-absorbance spectroscopy, ANS fluorescence spectroscopy, CD spectroscopy, TEM sample preparation and cryogenic freezing, gels preparation, gel adsorption experiments, cell culture and XRD/SAXS sample preparation; T.L performed the confocal microscopy and contributed to the CD spectroscopy and CAC measurements. Z.A measured the peptide content. G.Y performed the SAXS measurements and analysis; R.B contributed to the SAXS spectra analysis and rheology analysis; I.K performed the MD simulations; R.J, R.B and H.R supervised the research; E.A and H.R. wrote the manuscript. All authors have given approval to the final version of the manuscript.

Conflicts of interests

There are no conflicts to declare for all authors.

REFERENCES

1. Aizen, R., Tao, K., Rencus-Lazar, S., and Gazit, E. (2018). Functional metabolite assemblies—a review. J. Nanoparticle Res. *20*. 10.1007/s11051-018-4217-3.

2. Schweighauser, M., Shi, Y., Tarutani, A., Kametani, F., Murzin, A.G., Ghetti, B., Matsubara, T., Tomita, T., Ando, T., Hasegawa, K., et al. (2020). Structures of α-synuclein filaments from multiple system atrophy. Nat. 2020 5857825 *585*, 464–469. 10.1038/s41586-020-2317-6.

3. Cohen-Erez, I., and Rapaport, H. (2015). Coassemblies of the Anionic Polypeptide γ-PGA and Cationic β-Sheet Peptides for Drug Delivery to Mitochondria. Biomacromolecules *16*, 3827–3835. 10.1021/acs.biomac.5b01140.

4. Zhang, Y., Lu, F., Yager, K.G., Van Der Lelie, D., and Gang, O. (2013). A general strategy for the DNA-mediated self-assembly of functional nanoparticles into heterogeneous systems. Nat. Nanotechnol. *8*, 865–872. 10.1038/nnano.2013.209.

5. Aggeli, A., Nyrkova, I.A., Bell, M., Harding, R., Carrick, L., McLeish, T.C.B., Semenov, A.N., and Boden, N. (2001). Hierarchical self-assembly of chiral rod-like molecules as a model for peptide β-sheet tapes, ribbons, fibrils, and fibers. Proc. Natl. Acad. Sci. U. S. A. *98*, 11857–11862. 10.1073/pnas.191250198.

6. Xiao, L., Zhao, D., Chan, W.-H., Choi, M.M.F., and Li, H.-W. (2010). Inhibition of beta 1–40 amyloid fibrillation with N-acetyl-l-cysteine capped quantum dots. Biomaterials *31*, 91–98. 10.1016/J.BIOMATERIALS.2009.09.014.

7. Tian, Y., Zhang, Y., Wang, T., Xin, H.L., Li, H., and Gang, O. (2016). Lattice engineering through nanoparticle-DNA frameworks. Nat. Mater. *15*, 654–661. 10.1038/nmat4571.

8. Issa, A., Izquierdo, I., Merheb, M., Ge, D., Broussier, A., Ghabri, N., Marguet, S., Couteau, C., Bachelot, R., and Jradi, S. (2021). One Strategy for Nanoparticle Assembly onto 1D, 2D, and 3D Polymer Micro and Nanostructures. ACS Appl. Mater. Interfaces *13*, 41846–41856. 10.1021/acsami.1c03905.

9. Gazit, E. (2007). Self-assembled peptide nanostructures: the design of molecular building blocks and their technological utilization. Chem. Soc. Rev. *36*, 1263. 10.1039/b605536m.

10. Zhao, X., and Zhang, S. (2004). Fabrication of molecular materials using peptide construction motifs. Trends Biotechnol. *22*, 470–476. 10.1016/j.tibtech.2004.07.011.

11. Lakshmanan, A., Zhang, S., and Hauser, C.A.E. (2012). Short self-assembling peptides as building blocks for modern nanodevices. Trends Biotechnol. *30*, 155–165. 10.1016/j.tibtech.2011.11.001.

12. Bowerman, C.J., and Nilsson, B.L. (2012). Self-assembly of amphipathic β-sheet peptides: Insights and applications. Pept. Sci. *98*, 169–184. 10.1002/bip.22058.

13. Wittung, P., Eriksson, M., Lyng, R., Nielsen, P.E., and Norden, B. (1995). Induced Chirality in PNA-PNA Duplexes. J. Am. Chem. Soc. *117*, 10167–10173. 10.1021/ja00146a001.

14. Amosi, N., Zarzhitsky, S., Gilsohn, E., Salnikov, O., Monsonego-Ornan, E., Shahar, R., and Rapaport, H. (2012). Acidic peptide hydrogel scaffolds enhance calcium phosphate mineral turnover into bone tissue. Acta Biomater. *8*, 2466–2475. 10.1016/j.actbio.2012.04.003.

15. Zarzhitsky, S., Edri, H., Azoulay, Z., Cohen, I., Ventura, Y., Gitelman, A., and Rapaport, H. (2013). The effect of pH and calcium ions on the stability of amphiphilic and anionic β-sheet

peptide hydrogels. Pept. Sci. *100*, 760–772. 10.1002/bip.22282.

16. Fichman, G., and Gazit, E. (2014). Self-assembly of short peptides to form hydrogels: Design of building blocks, physical properties and technological applications. Acta Biomater. *10*, 1671–1682. 10.1016/j.actbio.2013.08.013.

17. Mandel-Gutfreund, Y., and Gregoret, L.M. (2002). On the significance of alternating patterns of polar and non-polar residues in beta-strands. J. Mol. Biol. *323*, 453–461. 10.1016/S0022-2836(02)00973-7.

18. DeGrado, W.F., Wasserman, Z.R., and Lear, J.D. (1989). Protein design, a minimalist approach. Science (80-.). *243*, 622–628. 10.1126/science.2464850.

19. Ulijn, R. V., and Smith, A.M. (2008). Designing peptide based nanomaterials. Chem. Soc. Rev. *37*, 664. 10.1039/b609047h.

20. Baruch Leshem, A., Zarzhitsky, S., and Rapaport, H. (2015). Functional Peptide Monolayers at Interfaces. Isr. J. Chem. *55*, 661–670. 10.1002/ijch.201400172.

21. Bera, S., Mondal, S., Tang, Y., Jacoby, G., Arad, E., Guterman, T., Jelinek, R., Beck, R., Wei, G., and Gazit, E. (2019). Deciphering the Rules for Amino Acid Co-Assembly Based on Interlayer Distances. ACS Nano *13*, 1703–1712. 10.1021/acsnano.8b07775.

22. Gazit, E. (2002). A possible role for pi-stacking in the self-assembly of amyloid fibrils. FASEB J. *16*, 77–83. 10.1096/fj.01-0442hyp.

23. Rhys, G.G., Dawson, W.M., Beesley, J.L., Martin, F.J.O., Brady, R.L., Thomson, A.R., and Woolfson, D.N. (2021). How coiled-coil assemblies accommodate multiple aromatic residues. Biomacromolecules *22*, 2010–2019. 10.1021/acs.biomac.1c00131.

24. Kumar, P., Paterson, N.G., Clayden, J., and Woolfson, D.N. (2022). De novo design of discrete, stable 310-helix peptide assemblies. Nature *607*, 387–392. 10.1038/s41586-022-04868-x.

25. Rha, A.K., Das, D., Taran, O., Ke, Y., Mehta, A.K., and Lynn, D.G. (2020). Electrostatic Complementarity Drives Amyloid/Nucleic Acid Co-Assembly. Angew. Chemie - Int. Ed. *59*, 358–363. 10.1002/anie.201907661.

26. Yosefi, G., Levi, T., Rapaport, H., and Bitton, R. (2020). Time matters for macroscopic membranes formed by alginate and cationic β-sheet peptides. Soft Matter *16*, 10132–10142. 10.1039/d0sm01197e.

27. Yu, Z., Erbas, A., Tantakitti, F., Palmer, L.C., Jackman, J.A., De La Cruz, M.O., Cho, N.J., and Stupp, S.I. (2017). Co-assembly of Peptide Amphiphiles and Lipids into Supramolecular Nanostructures Driven by Anionâ'Ï€ Interactions. J. Am. Chem. Soc. *139*, 7823–7830. 10.1021/jacs.7b02058.

28. Fichman, G., Adler-Abramovich, L., Manohar, S., Mironi-Harpaz, I., Guterman, T., Seliktar, D., Messersmith, P.B., and Gazit, E. (2014). Seamless metallic coating and surface adhesion of self-assembled bioinspired nanostructures based on Di-(3,4-dihydroxy- l -phenylalanine) peptide motif. ACS Nano *8*, 7220–7228. 10.1021/nn502240r.

29. Shlomo, Z., Vinod, T.P., Jelinek, R., and Rapaport, H. (2015). Stacking interactions by two Phe side chains stabilize and orient assemblies of even the minimal amphiphilic β-sheet motif. Chem. Commun. *51*, 3154–3157. 10.1039/c4cc09673h.

30. Tikhonova, T.N., Rovnyagina, N.N., Arnon, Z.A., Yakimov, B.P., Efremov, Y.M., Cohen-

Gerassi, D., Halperin-Sternfeld, M., Kosheleva, N. V, Drachev, V.P., Svistunov, A.A., et al. (2021). Mechanical Enhancement and Kinetics Regulation of Fmoc-Diphenylalanine Hydrogels by Thioflavin T. Angew. Chemie Int. Ed. *60*, 25339–25345. 10.1002/anie.202107063.

31. Guo, C., Arnon, Z.A., Qi, R., Zhang, Q., Adler-Abramovich, L., Gazit, E., and Wei, G. (2016). Expanding the Nanoarchitectural Diversity Through Aromatic Di- and Tri-Peptide Coassembly: Nanostructures and Molecular Mechanisms. ACS Nano *10*. 10.1021/acsnano.6b02739.

32. Chakraborty, P., Tang, Y., Guterman, T., Arnon, Z.A., Yao, Y., Wei, G., and Gazit, E. (2020). Co-Assembly between Fmoc Diphenylalanine and Diphenylalanine within a 3D Fibrous Viscous Network Confers Atypical Curvature and Branching. Angew. Chemie Int. Ed. *59*, 23731–23739. 10.1002/anie.202009488.

33. Guo, J., Rich-New, S.T., Liu, C., Huang, Y., Tan, W., He, H., Yi, M., Zhang, X., Egelman, E.H., Wang, F., et al. (2023). Hierarchical assembly of intrinsically disordered short peptides. Chem, 1–17. 10.1016/j.chempr.2023.04.023.

34. Lutz, J.F., Lehn, J.M., Meijer, E.W., and Matyjaszewski, K. (2016). From precision polymers to complex materials and systems. Nat. Rev. Mater. *1*. 10.1038/natrevmats.2016.24.

35. Thota, C.K., Berger, A.A., Elomaa, L., Nie, C., Böttcher, C., and Koksch, B. (2020). Coassembly Generates Peptide Hydrogel with Wound Dressing Material Properties. ACS Omega *5*, 8557–8563. 10.1021/acsomega.9b04371.

36. Oren, O., Ben Zichri, S., Taube, R., Jelinek, R., and Papo, N. (2020). Aβ42 Double Mutant Inhibits Aβ42-Induced Plasma and Mitochondrial Membrane Disruption in Artificial Membranes, Isolated Organs, and Intact Cells. ACS Chem. Neurosci. *11*, 1027–1037. 10.1021/acschemneuro.9b00638.

37. Taş, K., Volta, B.D., Lindner, C., El Bounkari, O., Hille, K., Tian, Y., Puig-Bosch, X., Ballmann, M., Hornung, S., Ortner, M., et al. (2022). Designed peptides as nanomolar cross-amyloid inhibitors acting via supramolecular nanofiber co-assembly. Nat. Commun. *13*. 10.1038/s41467-022-32688-0.

38. Azoulay, Z., and Rapaport, H. (2016). The assembly state and charge of amphiphilic β-sheet peptides affect blood clotting. J. Mater. Chem. B *4*, 3859–3867. 10.1039/C6TB00330C.

39. Ghosh, M., Bera, S., Schiffmann, S., Shimon, L.J.W., and Adler-Abramovich, L. (2020). Collagen-Inspired Helical Peptide Coassembly Forms a Rigid Hydrogel with Twisted Polyproline II Architecture. ACS Nano *14*, 9990–10000. 10.1021/acsnano.0c03085.

40. Merg, A.D., Touponse, G., Genderen, E. Van, Blum, T.B., Zuo, X., Bazrafshan, A., Siaw, H.M.H., McCanna, A., Brian Dyer, R., Salaita, K., et al. (2020). Shape-Shifting Peptide Nanomaterials: Surface Asymmetry Enables pH-Dependent Formation and Interconversion of Collagen Tubes and Sheets. J. Am. Chem. Soc. *142*, 19956–19968. 10.1021/jacs.0c08174.

41. Cheng, D., Chen, X., Zhang, W., Guo, P., Xue, W., Xia, J., Wu, S., Shi, J., Ma, D., Zuo, X., et al. (2023). Design of Multicomponent Peptide Fibrils with Ordered and Programmable Compositional Patterns. Angew. Chemie Int. Ed. 10.1002/anie.202303684.

42. Wong, K.M., Robang, A.S., Lint, A.H., Wang, Y., Dong, X., Xiao, X., Seroski, D.T., Liu, R., Shao, Q., Hudalla, G.A., et al. (2021). Engineering β-Sheet Peptide Coassemblies for Biomaterial Applications. J. Phys. Chem. B *125*, 13599–13609. 10.1021/acs.jpcb.1c04873.

43. Swanekamp, R.J., Dimaio, J.T.M., Bowerman, C.J., and Nilsson, B.L. (2012). Coassembly of enantiomeric amphipathic peptides into amyloid-inspired rippled β-sheet fibrils. J. Am. Chem.

Soc. *134*, 5556–5559. 10.1021/ja301642c.

44. Garcia, A.M., Iglesias, D., Parisi, E., Styan, K.E., Waddington, L.J., Deganutti, C., De Zorzi, R., Grassi, M., Melchionna, M., Vargiu, A. V., et al. (2018). Chirality Effects on Peptide Self-Assembly Unraveled from Molecules to Materials. Chem, 1–15. 10.1016/j.chempr.2018.05.016.

45. Rufo, C.M., Moroz, Y.S., Moroz, O. V., Stöhr, J., Smith, T. a., Hu, X., Degrado, W.F., and Korendovych, I. V. (2014). Short peptides self-assemble to produce catalytic amyloids. Nat. Chem. *6*, 303–309. 10.1038/nchem.1894.

46. Rout, S.K., Friedmann, M.P., Riek, R., and Greenwald, J. (2018). A prebiotic template-directed peptide synthesis based on amyloids. Nat. Commun. *9*. 10.1038/s41467-017-02742-3.

47. Wang, M., Lv, Y., Liu, X., Qi, W., Su, R., and He, Z. (2016). Enhancing the Activity of Peptide-Based Artificial Hydrolase with Catalytic Ser/His/Asp Triad and Molecular Imprinting. ACS Appl. Mater. Interfaces *8*, 14133–14141. 10.1021/acsami.6b04670.

48. Ardona, H.A.M., Draper, E.R., Citossi, F., Wallace, M., Serpell, L.C., Adams, D.J., and Tovar, J.D. (2017). Kinetically Controlled Coassembly of Multichromophoric Peptide Hydrogelators and the Impacts on Energy Transport. J. Am. Chem. Soc. *139*, 8685–8692. 10.1021/jacs.7b04006.

49. Singh, N., Tena-Solsona, M., Miravet, J.F., and Escuder, B. (2015). Towards Supramolecular Catalysis with Small Self-assembled Peptides. Isr. J. Chem. *55*, 711–723. 10.1002/ijch.201400185.

50. Inostroza-Brito, K.E., Collin, E., Siton-Mendelson, O., Smith, K.H., Monge-Marcet, A., Ferreira, D.S., Rodríguez, R.P., Alonso, M., Rodríguez-Cabello, J.C., Reis, R.L., et al. (2015). Co-Assembly, spatiotemporal control and morphogenesis of a hybrid protein-peptide system. Nat. Chem. *7*, 897–904. 10.1038/nchem.2349.

51. Green, H., Ochbaum, G., Gitelman-Povimonsky, A., Bitton, R., and Rapaport, H. (2018). RGD-presenting peptides in amphiphilic and anionic β-sheet hydrogels for improved interactions with cells. RSC Adv. *8*, 10072–10080. 10.1039/c7ra12503h.

52. Arad, E., Malishev, R., Rapaport, H., and Jelinek, R. (2018). Membrane Determinants Affect Fibrillation Processes of β-Sheet Charged Peptides. Biomacromolecules *19*, 307–314. 10.1021/acs.biomac.7b01318.

53. Seroski, D.T., Dong, X., Wong, K.M., Liu, R., Shao, Q., Paravastu, A.K., Hall, C.K., and Hudalla, G.A. (2020). Charge guides pathway selection in β-sheet fibrillizing peptide co-assembly. Commun. Chem. *3*. 10.1038/s42004-020-00414-w.

54. Shao, Q., Wong, K.M., Seroski, D.T., Wang, Y., Liu, R., Paravastu, A.K., Hudalla, G.A., and Hall, C.K. (2020). Anatomy of a selectively coassembled β-sheet peptide nanofiber. Proc. Natl. Acad. Sci. U. S. A. *117*, 4710–4717. 10.1073/pnas.1912810117.

55. Hamsici, S., White, A.D., and Acar, H. (2022). Peptide framework for screening the effects of amino acids on assembly. Sci. Adv. *8*, 1–14. 10.1126/sciadv.abj0305.

56. Soto Morales, B., Liu, R., Olguin, J., Ziegler, A.M., Herrera, S.M., Backer-Kelley, K.L., Kelley, K.L., and Hudalla, G.A. (2021). Injectable nanofibrillar hydrogels based on charge-complementary peptide co-assemblies. Biomater. Sci. *9*, 2494–2507. 10.1039/D0BM01372B.

57. Tena-Solsona, M., Alonso-de Castro, S., Miravet, J.F., and Escuder, B. (2014). Co-assembly of tetrapeptides into complex pH-responsive molecular hydrogel networks. J. Mater. Chem. B *2*,

6192–6197. 10.1039/C4TB00795F.

58. Redondo-Gómez, C., Abdouni, Y., Becer, C.R., and Mata, A. (2019). Self-Assembling Hydrogels Based on a Complementary Host–Guest Peptide Amphiphile Pair. Biomacromolecules *20*, 2276–2285. 10.1021/acs.biomac.9b00224.

59. Raymond, D.M., and Nilsson, B.L. (2018). Multicomponent peptide assemblies. Chem. Soc. Rev. *47*, 3659–3720. 10.1039/C8CS00115D.

60. Toksoz, S., Mammadov, R., Tekinay, A.B., and Guler, M.O. (2011). Electrostatic effects on nanofiber formation of self-assembling peptide amphiphiles. J. Colloid Interface Sci. *356*, 131–137. 10.1016/j.jcis.2010.12.076.

61. Edwards, W., and Smith, D.K. (2014). Enantioselective Component Selection in Multicomponent Supramolecular Gels. J. Am. Chem. Soc. *136*, 1116–1124. 10.1021/ja411724r.

62. Liu, R., Dong, X., Seroski, D.T., Soto Morales, B., Wong, K.M., Robang, A.S., Melgar, L., Angelini, T.E., Paravastu, A.K., Hall, C.K., et al. (2023). Side-Chain Chemistry Governs Hierarchical Order of Charge-Complementary β-sheet Peptide Coassemblies. Angew. Chemie Int. Ed. *62*. 10.1002/anie.202314531.

63. Rapaport, H., Kjaer, K., Jensen, T.R., Leiserowitz, L., and Tirrell, D.A. (2000). Two-Dimensional Order in β-Sheet Peptide Monolayers. J. Am. Chem. Soc. *122*, 12523–12529. 10.1021/ja002238t.

64. Rapaport, H., Grisaru, H., and Silberstein, T. (2008). Hydrogel scaffolds of amphiphilic and acidic ??-sheet peptides. Adv. Funct. Mater. *18*, 2889–2896. 10.1002/adfm.200800117.

65. Isenberg, H., Kjaer, K., and Rapaport, H. (2006). Elasticity of Crystalline β-Sheet Monolayers. J. Am. Chem. Soc. *128*, 12468–12472. 10.1021/ja062363q.

66. Zarzhitsly, S., and Rapaport, H. (2011). The interactions between doxorubicin and amphiphilic and acidic β-sheet peptides towards drug delivery hydrogels. J. Colloid Interface Sci., 525–531.

67. Rapaport, H., Grisaru, H., and Silberstein, T. (2008). Hydrogel scaffolds of amphiphilic and acidic β-sheet peptides. Adv. Funct. Mater. *18*, 2889–2896. 10.1002/adfm.200800117.

68. Segman-Magidovich, S., Grisaru, H., Gitli, T., Levi-Kalisman, Y., and Rapaport, H. (2008). Matrices of acidic ??-sheet peptides as templates for calcium phosphate mineralization. Adv. Mater. *20*, 2156–2161. 10.1002/adma.200702125.

69. Ben Ghedalia-Peled, N., Cohen-Erez, I., Rapaport, H., and Vago, R. (2021). Aggressiveness of 4T1 breast cancer cells hampered by Wnt production-2 inhibitor nanoparticles: An in vitro study. Int. J. Pharm. *596*, 120208. 10.1016/j.ijpharm.2021.120208.

70. Cohen-Erez, I., Harduf, N., and Rapaport, H. (2019). Oligonucleotide loaded polypeptide-peptide nanoparticles towards mitochondrial-targeted delivery. Polym. Adv. Technol. *30*, 2506–2514. 10.1002/pat.4707.

71. Charles, C., Cohen-Erez, I., Kazaoka, B., Melnikov, O., Stein, D.E., Sensenig, R., Rapaport, H., and Orynbayeva, Z. (2020). Mitochondrial responses to organelle-specific drug delivering nanoparticles composed of polypeptide and peptide complexes. Nanomedicine *15*, 2917–2932. 10.2217/nnm-2020-0266.

72. Lopes, J.L.S., Miles, A.J., Whitmore, L., and Wallace, B.A. (2014). Distinct circular dichroism spectroscopic signatures of polyproline II and unordered secondary structures: Applications in

secondary structure analyses. Protein Sci. *23*, 1765–1772. 10.1002/pro.2558.

73. Tsai, C.L., Wu, S.Y., Hsu, H.K., Huang, S.B., Lin, C.H., Chan, Y.T., and Wang, S.K. (2021). Preparation and conformational analysis of polyproline tri-helix macrocycle nanoscaffolds of varied sizes. Nanoscale *13*, 4592–4601. 10.1039/d0nr08184a.

74. Yosefi, G., Cohen-Erez, I., Nativ-Roth, E., Rapaport, H., and Bitton, R. (2020). Spontaneous Alignment of Self-Assembled Cationic and Amphiphilic β-Sheet Peptides. Adv. Mater. Interfaces *7*, 2000332. 10.1002/admi.202000332.

75. Arad, E., Green, H., Jelinek, R., and Rapaport, H. (2020). Revisiting thioflavin T (ThT) fluorescence as a marker of protein fibrillation – The prominent role of electrostatic interactions. J. Colloid Interface Sci. *573*, 87–95. 10.1016/j.jcis.2020.03.075.

76. Sajid, J., Elhaddaoui, A., and Turrell, S. (1997). Investigation of the binding of congo red to amyloid in Alzheimer's diseased tissue. J. Mol. Struct. *408–409*, 181–184. 10.1016/S0022-2860(96)09669-X.

77. Yermiyahu, Z., Lapides, I., and Yariv, S. (2007). Thermo-visible-absorption spectroscopy study of the protonated Congo-red montmorillonite complex. Appl. Clay Sci. *37*, 1–11. 10.1016/j.clay.2006.10.006.

78. Milanesi, M., Brotzakis, Z.F., and Vendruscolo, M. (2024). Transient interactions between the fuzzy coat and the cross- b core of brain-derived beta-amyloid filaments https://doi.org/10.1101/2024.01.08.574772.

79. Wegmann, S., Medalsy, I.D., Mandelkow, E., and Müller, D.J. (2012). The fuzzy coat of pathological human Tau fibrils is a two-layered polyelectrolyte brush. Proc. Natl. Acad. Sci. U. S. A. *110*, E313–E321. 10.1073/pnas.1212100110.

80. Ulamec, S.M., Brockwell, D.J., and Radford, S.E. (2020). Looking Beyond the Core: The Role of Flanking Regions in the Aggregation of Amyloidogenic Peptides and Proteins. Front. Neurosci. *14*, 1–23. 10.3389/fnins.2020.611285.

81. Prilusky, J., Hodis, E., Canner, D., Decatur, W.A., Oberholser, K., Martz, E., Berchanski, A., Harel, M., and Sussman, J.L. (2011). Proteopedia: A status report on the collaborative, 3D web-encyclopedia of proteins and other biomolecules. J. Struct. Biol. *175*, 244–252. 10.1016/j.jsb.2011.04.011.

82. Harms, M.J., Schlessman, J.L., Chimenti, M.S., Sue, G.R., Damjanović, A., and García-Moreno E., B. (2008). A buried lysine that titrates with a normal pKa: Role of conformational flexibility at the protein-water interface as a determinant of pKavalues. Protein Sci. *17*, 833–845. 10.1110/ps.073397708.

83. Urry, D.W., Gowda, D.C., Peng, S., Parker, T.M., Jing, N., and Harris, R.D. (1994). Nanometric design of extraordinary hydrophobic-induced pKa shifts for aspartic acid: Relevance to protein mechanisms. Biopolymers *34*, 889–896. 10.1002/bip.360340708.

84. Pahari, S., Sun, L., and Alexov, E. (2019). PKAD: a database of experimentally measured pKa values of ionizable groups in proteins. Database *2019*. 10.1093/database/baz024.

85. Freyer, M.W., and Lewis, E.A. (2008). Isothermal Titration Calorimetry: Experimental Design, Data Analysis, and Probing Macromolecule/Ligand Binding and Kinetic Interactions. In Methods in Cell Biology, pp. 79–113. 10.1016/S0091-679X(07)84004-0.

86. Lounis, F.M., Chamieh, J., Leclercq, L., Gonzalez, P., Geneste, A., Prelot, B., and Cottet, H.

(2017). Interactions between Oppositely Charged Polyelectrolytes by Isothermal Titration Calorimetry: Effect of Ionic Strength and Charge Density. J. Phys. Chem. B *121*, 2684–2694. 10.1021/acs.jpcb.6b11907.

87. Trapaidze, A., Hureau, C., Bal, W., Winterhalter, M., and Faller, P. (2012). Thermodynamic study of Cu2+ binding to the DAHK and GHK peptides by isothermal titration calorimetry (ITC) with the weaker competitor glycine. JBIC J. Biol. Inorg. Chem. *17*, 37–47. 10.1007/s00775-011-0824-5.

88. Sathaye, S., Mbi, A., Sonmez, C., Chen, Y., Blair, D.L., Schneider, J.P., and Pochan, D.J. (2015). Rheology of peptide- and protein-based physical hydrogels: Are everyday measurements just scratching the surface? Wiley Interdiscip. Rev. Nanomedicine Nanobiotechnology *7*, 34–68. 10.1002/wnan.1299.

89. Rapaport, H. (2006). Ordered Peptide Assemblies at Interfaces. Supramol. Chem. *18*, 445–454. 10.1080/10610270600665905.

90. Sneer, R., Weygand, M.J., Kjaer, K., Tirrell, D.A., and Rapaport, H. (2004). Parallelβ-Sheet Assemblies at Interfaces. ChemPhysChem *5*, 747–750. 10.1002/cphc.200301046.

91. Schneider, A., Lang, A., and Naumann, W. (2010). Fluorescence spectroscopic determination of the critical aggregation concentration of the GnRH antagonists Cetrorelix, Teverelix and Ozarelix. J. Fluoresc. *20*, 1233–1240. 10.1007/s10895-010-0674-5.

92. Younan, N.D., and Viles, J.H. (2015). A Comparison of Three Fluorophores for the Detection of Amyloid Fibers and Prefibrillar Oligomeric Assemblies. ThT (Thioflavin T); ANS (1-Anilinonaphthalene-8-sulfonic Acid); and bisANS (4,4′-Dianilino-1,1′-binaphthyl-5,5′-disulfonic Acid). Biochemistry *54*, 4297–4306. 10.1021/acs.biochem.5b00309.

93. Xing, Y., Nandakumar, A., Kakinen, A., Sun, Y., Davis, T.P., Ke, P.C., and Ding, F. (2021). Amyloid Aggregation under the Lens of Liquid-Liquid Phase Separation. J. Phys. Chem. Lett. *12*, 368–378. 10.1021/acs.jpclett.0c02567.

94. Frid, P., Anisimov, S. V., and Popovic, N. (2007). Congo red and protein aggregation in neurodegenerative diseases. Brain Res. Rev. *53*, 135–160. 10.1016/j.brainresrev.2006.08.001.

95. Hodis, E., Prilusky, J., Martz, E., Silman, I., Moult, J., and Sussman, J.L. (2008). Proteopedia - A scientific "wiki" bridging the rift between three-dimensional structure and function of biomacromolecules. Genome Biol. *9*, 121.1-121.10. 10.1186/gb-2008-9-8-r121.

TOC Figure